Stem Cells Translational Medicine, 2022, **11**, 1072–1088
https://doi.org/10.1093/stcltm/szac052
Advance access publication 1 October 2022
Original Research

Preclinical Study of Human Bone Marrow-Derived Mesenchymal Stem Cells Using a 3-Dimensional Manufacturing Setting for Enhancing Spinal Fusion

Sumin Cho[1,2,†], Hyemin Choi[3,†], Hyundoo Jeong[1], Su Yeon Kwon[3], Eun Ji Roh[3], Kwang-Hun Jeong[1,2], Inho Baek[4], Byoung Ju Kim[4], Soo-Hong Lee[4], Inbo Han[*,3], Jae Min Cha[*,1,2]

[1]Department of Mechatronics Engineering, College of Engineering, Incheon National University, Incheon, Republic of Korea
[2]3D Stem Cell Bioengineering Laboratory, Research Institute for Engineering and Technology, Incheon National University, Incheon, Republic of Korea
[3]Department of Neurosurgery, CHA University School of Medicine, CHA Bundang Medical Center, Seongnam-si, Gyeonggi-do, Republic of Korea
[4]Department of Biomedical Technology, Dongguk University, Goyang-si, Gyeonggi-do, Republic of Korea

[*]Corresponding author: Inbo Han, Department of Neurosurgery, CHA University School of Medicine, CHA Bundang Medical Center, Seongnam-si, Gyeonggi-do 13496, Republic of Korea. Email: hanib@cha.ac.kr; Jae Min Cha, Department of Mechatronics Engineering, College of Engineering, Incheon National University, Incheon 22012, Republic of Korea. j.cha@inu.ac.kr
[†]Contributed equally.

Abstract

Spinal fusion surgery is a surgical technique that connects one or more vertebrae at the same time to prevent movement between the vertebrae. Although synthetic bone substitutes or osteogenesis-inducing recombinant proteins were introduced to promote bone union, the rate of revision surgery is still high due to pseudarthrosis. To promote successful fusion after surgery, stem cells with or without biomaterials were introduced; however, conventional 2D-culture environments have resulted in a considerable loss of the innate therapeutic properties of stem cells. Therefore, we conducted a preclinical study applying 3D-spheroids of human bone marrow-dewrived mesenchymal stem cells (MSCs) to a mouse spinal fusion model. First, we built a large-scale manufacturing platform for MSC spheroids, which is applicable to good manufacturing practice (GMP). Comprehensive biomolecular examinations, which include liquid chromatography-mass spectrometry and bioinformatics could suggest a framework of quality control (QC) standards for the MSC spheroid product regarding the identity, purity, viability, and potency. In our animal study, the mass-produced and quality-controlled MSC spheroids, either undifferentiated or osteogenically differentiated were well-integrated into decorticated bone of the lumbar spine, and efficiently improved angiogenesis, bone regeneration, and mechanical stability with statistical significance compared to 2D-cultured MSCs. This study proposes a GMP-applicable bioprocessing platform and QC directions of MSC spheroids aiming for their clinical application in spinal fusion surgery as a new bone graft substitute.

Key words: spinal fusion; mesenchymal stem cell; spheroid; bone regeneration; bioprocessing; quality control.

Graphical Abstract

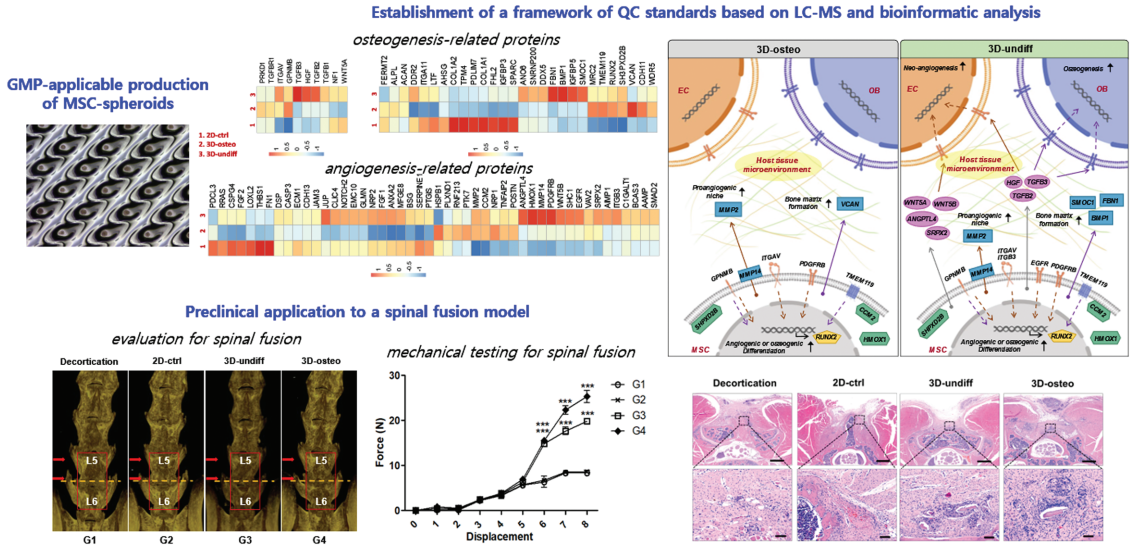

Received: 1 December 2021; Accepted: 12 June 2022.

Significance Statement

This study includes the development of a simple and cost-effective GMP-applicable bioprocessing platform capable of the large-scale manufacture of therapeutic MSC spheroids with high lot-to-lot consistency and a framework of the QC standards and relevant assay methods established with a support of thorough protein profiling analyses using LC-MS and bioinformatics. A mouse spinal fusion model was also developed, with the optimized delivery and surgery methods for MSC spheroids utilizing clinically approved gelatin sponge scaffolds and successfully enhanced spinal fusion efficacy with robust mechanical stability. This preclinical study will pave the way for the therapy to spinal fusion surgery.

Introduction

Spinal fusion surgery is performed to improve spinal stability by connecting 2 or more vertebrae in cases of vertebral fractures, severe spinal stenosis, or severe scoliosis. Pseudarthrosis (unsuccessful fusion) is a serious complication of spinal fusion surgery and is an important cause of postoperative pain, neurological disturbance, and reoperation.[1-4] To increase the success rate of spinal fusion, various synthetic bone substitutes, such as hydroxyapatites, tricalcium phosphate, and bioactive glass and biological factors, such as recombinant human bone morphogenetic protein-2 (rhBMP2) were introduced during the last decades.[2,5-8] According to a systematic review related to use of rhBMP2 in stand-alone lateral lumbar interbody fusion, it has been reported that the fusion rate (87.7%) with rhBMP2 was higher than that of studies without rhBMP2 (83.9%).[9] However, in their study, the overall complication rate was 42.2%, of which 11.1% required revision surgery. Among the reoperation cases, 20.4% was due to pseudarthrosis.[9] To address the limitations of currently available bone graft substitutes, the major strategy is to use stem cells alone or in combination with various biomaterials.[1,3,10-15] By searching on "clinicaltrials.gov" with the keywords "spinal fusion" and "stem cell," 10 registered trials were identified, and it was revealed that progenitor cells derived from the bone marrow are the most widely used among diverse progenitor cell populations. Furthermore, a comparison study of human mesenchymal stem cells (MSCs) derived from different sources, such as bone marrow, umbilical cord blood, placenta, and adipose tissue reported that MSCs derived from the bone marrow demonstrated extraordinary osteogenic potential along with the greatest immune-suppressive capability among all types of MSCs.[16]

MSCs have exhibited versatile therapeutic capabilities in a number of clinical trials due to their innate tropism migrating toward the inflamed and/or ischemic sites (homing), their immunomodulatory properties, and their exceptional regenerative properties to trigger endogenous repair programs by activating other stem or progenitor cells residing in the injured tissue and stimulating neo-angiogenesis.[17-20] Unlike other cell therapies which generally aim to replace damaged areas of the tissue, the therapeutic mechanism of action of MSCs is attributed mostly to the alteration of the tissue microenvironment via paracrine effector–induced secretion of various soluble bioactive molecules that promote immunomodulatory and/or regenerative activities of the host tissues, and the effects may persist for a long time even after the injected MSCs disappear.[21,22] However, many earlier studies reported that such properties of MSCs to secrete a mixture of therapeutic molecules hardly reproduces in a conventional monolayer culture condition where the individual cells grow on limited 2-dimensional (2D) borders and the native 3-dimensional (3D) interactions between cells and either the extracellular matrix (ECM) or other neighboring cells are disrupted. Contrastingly, MSCs self-assembled as multicellular aggregates can form closer 3D cellular associations with highly cumulated signaling molecules, which can create a microenvironment similar to that observed in vivo than in monolayer cultures.[23-25] Numerous studies have reported that the formation of 3D MSC aggregates could highly preserve the innate phenotype and properties of the MSCs, and thus efficiently reinforce their therapeutic efficacy by intensifying the differentiation potential, ECM secretion rate, immunomodulatory and angiogenic capacities, and survival rates after transplantation.[24-29] In our earlier study, we developed a microwell array culture system with a unique feature, which could completely circumvent wasting expensive stem cell material during the large-scale formation and culture of 3D MSC spheroids, thereby contributing to significant cost-saving. This simple and efficient bioprocessing platform could achieve highly reproducible and precise control of the sizes and cell numbers of the MSC spheroids and minimize the uncertainty in cellular behaviors, which are possibly caused by heterogeneity in the spheroid specifications.[30] Furthermore, the mass-produced MSC spheroids exhibited a 100-fold higher secretion rate of extracellular vesicles compared to the 2D-cultured control group while loaded with abundant angiogenic and neurotrophic factors.[31]

In this study, we conducted a set of preclinical studies applying 3D-spheroids of human bone marrow-derived MSCs to a mouse spinal fusion model. Firstly, a simple and cost-effective good manufacturing practice (GMP)-applicable bioprocessing platform was developed, which is capable of the large-scale manufacture of therapeutic MSC spheroids ensuring lot-to-lot reproducibility. Secondly, a framework to establish the quality control standards of MSC spheroids and relevant assay methods was suggested with a support of thorough protein profiling analyses using liquid chromatography-mass spectrometry and bioinformatics. Finally, we developed a mouse spinal fusion model with the optimized delivery and surgery methods for MSC spheroids utilizing clinically approved gelatin sponge scaffolds and successfully enhanced spinal fusion efficacy with robust mechanical stability compared to the control group.

Materials and Methods

Cell Maintenance

Human bone marrow-derived MSCs (Lonza, Basel, Switzerland) were cultured in 100-mm culture dishes (Corning, Tewsburg, MA, USA) with growth medium. The growth medium was supplemented with 10% fetal bovine serum (FBS; Invitrogen, Carlsbad, CA, USA) and 1% antibiotic-antimycotic (anti-anti; Invitrogen) in Dulbecco's modified Eagle's medium with low glucose (DMEM; Invitrogen). When 70%-80% confluent, the adherent MSCs were detached with TrypLE (Life Technologies, Carlsbad, CA, USA), counted, and seeded at 4500 cells/cm^2. Cells were incubated and maintained in a 5% CO_2 atmosphere at 37 °C until passage 6.

MSC-Spheroid Formation and Culture Using Microwell Array

Mass production of MSC spheroids was efficiently achieved using a microwell array system (EZSphere, IWAKI, Japan) that is commercially available as well as GMP-applicable and amenable to an appropriate certificate of analysis. The microwell array system was designed based on a 6-well plate, a well of which contained 2400 microwells with diameter and depth of 500 and 200 μm, respectively. Therefore, 14 400 MSC spheroids could be produced simultaneously using a single microwell array system. The unique configuration of the microwell array could support the complete resistance to cell attachment on the surface and prevention of cell loss that is caused by laborious washing steps for the cells not entrapped within microwells after seeding.[30] Before cell seeding, the microwells were washed with phosphate-buffered saline (PBS, Cytiva, Marlborough, USA) and serum-free alpha minimum essential medium (α-MEM, Invitrogen) to eliminate bubbles in the microwell. Passage 6 of MSCs were seeded at 1×10^6 cells in a microwell array of the 6-well plate and cultured in the growth medium (a group named "3D-undiff") or in the osteogenic medium (a group named "3D-osteo"). The growth medium consisted of α-MEM (Invitrogen) supplemented with 10% FBS (Invitrogen) and 1% penicillin/streptomycin (Gemini, Sacramento, CA). Osteogenic medium consisted of growth medium supplemented with 50 μg/mL ascorbate-2-phosphate (Sigma-Aldrich, St. Louis, MO, USA), 10 mM β-glycerophosphate (Sigma), and 100 nM dexamethasone (Sigma). 2D-MSCs were seeded at a density of 4500 cells/cm^2 in a 100-mm culture dish and cultured in either growth (a group named "2D-ctrl") or osteogenic medium (specific culture days are indicated in corresponding methods and results). The culture media of the 2D-MSC and 3D-osteo groups were renewed every 4 days. For the 3D-undiff group, medium exchange was not conducted in case of 4 days of culture period. For further analysis, MSC spheroids were collected with medium from the microwell array and separated by centrifugation at 167 × *g* for 1 minutes at room temperature.

Measurement of the MSC-Spheroid Size Distribution

To measure the size distribution, MSC spheroids collected from the microwell array on day 7 were photographed using a microscope (Olympus, Tokyo, Japan). The particle size distribution analysis was conducted using ImageJ software. More than 100 MSC spheroids were measured in each group for analysis (n = 5).

Live and Dead Cell Viability

Cell viability was measured using a Live/Dead Viability/Cytotoxicity assay kit (Life Technologies) with MSC spheroids cultured for 7 days in the microwells. MSC spheroids were stained with calcein-AM and ethidium homodimer-1 according to the manufacturer's instructions and photographed using a fluorescent microscope (Olympus). Cell viability analysis was performed using Fiji application with ImageJ (*n* = 5).

DNA Quantification Assay

Cell numbers of MSC spheroids were determined using a CyQUANT cell proliferation assay (Molecular Probes, Eugene, OR, USA). Following the manufacturer's instructions, lysis buffer and CyQUANT GR dye in the kit were added to each sample and incubated for 5 minutes at room temperature in a dark room. The fluorescence of the samples was measured at a wavelength of 520 nm on a microplate reader (Tecan, Mannedorf, Switzerland) (*n* = 5).

Flow Cytometry Analysis

Cell surface antigens of positive MSC markers (CD44 and CD73) and negative MSC markers (CD45 and CD34) on human bone marrow-derived MSCs were detected by flow cytometry. The cells were washed twice with PBS, dissociated with 0.25% trypsin (Hyclone, Uppsala, Sweden), and then collected by centrifugation. The cell pellets were resuspended in PBS with 2% FBS (FACS buffer), incubated with the specific primary antibody for 30 minutes at 4 °C, and washed with FACS buffer 3 times. Antibodies against CD44 (CD44-PE, BioLegend, San Diego, CA, USA), CD73 (CD73-PE, BioLegend), CD45 (CD45-PE, BioLegend), and CD34 (CD34-PerCP, BioLegend) were used. The antibodies were used as 1:100 dilutions in FACS buffer. Cells were washed with FACS buffer 3 times, and fluorescence was detected using BD Accuri C6 (BD Science, USA) (*n* = 3).

Proteome Analysis

The fractionated peptides were loaded onto a trap column filled with Acclaim PepMap100 C18 resin (Thermo Fisher, Waltham, MA, USA). The peptides were eluted with a linear gradient from 5% to 30% of 0.1% formic acid in acetonitrile for over 120 minutes at a flow rate of 300 nL/minute, separated by an analytical column (75 μm × 15 cm, Thermo Fisher), and ionized by electrospray voltage of 2.4 kV. The mass spectrometer (MS) was operated using the top 10 data-dependent method. The MS scans were collected from 300 to 2000 *m/z* with 70 000 resolutions (at *m/z* 200 and 1×10^6 automatic gain control target). The top 10 intense peaks with a charge state ≥ 2 were selected for higher energy collisional dissociation collision with a normalized collision energy of 25%, and tandem mass spectra were collected at a resolution of 17 500 at 200 *m/z*. Database searching for protein identification and quantification was performed using Proteome Discoverer 2.2 software (Thermo Fisher). SEQUEST-HT was used to search against the UniProt database. The false discovery rate (FDR) of peptide identification was evaluated using database searching against the corresponding reversed database. Database search parameters included a precursor mass tolerance of 10 ppm, fragment ion mass tolerance of 0.02 Da, fixed modification for carbamidomethyl cysteine and variable modification for methionine oxidation, up to 2 missing cleavages, and N/Q deamination was set for the search. An FDR of less than 1% was obtained at the peptide level and filtered with high peptide confidence (*n* = 5).

Bioinformatic Analysis

To confirm the validity of the experimental results, we verified the abundance levels of proteins that are related to the bone regeneration mechanism. To leverage bioinformatics techniques, we first searched all Gene Ontology (GO) terms that are related to "osteoblast", "ossification", and "angiogenesis" by accessing EBI QuickGO, which is a web-based big data platform for the gene ontology and annotation (www.ebi.ac.uk/QuickGO/). Then, based on the automated text mining approach, we investigated the liquid chromatography–mass spectrometry (LC–MS) protein profile data and checked their GO annotation using text matching techniques (Supplementary Table S1). Next, we extracted proteins

that were annotated to the aforementioned GO terms and compared their abundance levels using log-transformed mean values. Since the protein abundance level in each experimental group showed relatively large differences, direct comparison of the protein abundance level makes it difficult to unveil the relative changing patterns of protein abundance levels in each experimental group. To show balanced and clear patterns, we obtained the average protein abundance level for each group and performed log2 transformation (ie, log2 (1+ protein abundance level)). Then, to normalize the protein abundance level, we obtained *z*-scores for each protein and visualized the protein abundance level for each experimental group using a heatmap and balloon plots. Note that the *z*-score is given by

$$z = \frac{x - \mu}{\sigma},$$

where x is the protein abundance level, and μ and σ are the mean and standard deviation of the protein abundance level across different samples, respectively. To effectively visualize the balloon plot, we divided the absolute protein abundance level by 10 000 000 and performed a log transformation. The heatmap can visualize the fold changes of the protein abundance levels, and the balloon plot can depict the absolute abundance level for each protein. Next, to verify the statistical significance of the proteins, we performed Student's *t* test for each pair of experimental groups and only retained proteins with *P*-values smaller than .05. Among these proteins with statistical significance, we kept the proteins with a fold change greater than 2 and compared their log-fold change and abundance level through balloon plots. Finally, we visualized the MSC-specific marker proteins using the same approach (Supplementary Table S2). We used the R package pheatmap (Pheatmap: pretty heatmaps."R package version 1.2, 2012), ggpubr (ggpubr R Package: ggplot2-Based Publication Ready Plots, 2020), and ggplot2 to visualize heat maps and balloon plots.[32]

Animals

Eight-week-old female C57BL/6 mice weighing 22 g were purchased from KoaTech (Pyeongtaek, Korea) and kept at 55%-65% humidity and a controlled temperature of 24 ± 3 °C with a 12 h/12 h light/dark cycle. All animals had ad libitum access to food and tap water. After 2 weeks of acclimatization, surgeries were performed. Mice were anesthetized intraperitoneally with a mixture of Zoletil (50 mg/kg; Virbac Labolatories, Carros, France) and Rompun (10 mg/kg; Bayer, Seoul, Korea). All animal procedures were performed in accordance with the protocol approved by the Institutional Animal Care and Use Committee (IACUC) of CHA University (IACUC200058).

Gelatin Sponge Scaffold Preparation

To prepare the gelatin sponge scaffolds, we first cut absorbable gelatin sponges (Cutanplast , Masciabrunelli, Milano, Italy) to 10 mm (length) × 7 mm (width) × 3 mm (height). Next, 6000 MSC spheroids (2.5×10^6 cells) were uniformly suspended in 50 μL of α-MEM and evenly seeded onto the sponge scaffolds. For MSCs cultured on 2D (2D-ctrl), MSCs cultured on the 2D culture plate for 3 days were collected and seeded onto the sponge scaffolds with the same cell number.

Mouse Spinal Fusion Model

Once the mice were anesthetized, skin and hair covering the surgical site were shaved with a blade, and the surgical site was sterilized with povidone–iodine and 70% ethanol. Animals were positioned in the prone position, with folded gauze placed under the abdomen to facilitate access and visibility of the surgical site. Posterolateral lumbar fusion was performed at the 5th to 6th lumbar vertebrae (L5-L6), as reported in earlier studies.[1,3] Briefly, a 2-cm midline incision was made in the skin at L5-L6. The paravertebral muscle covering the articular processes of L5-L6 was scraped with a #10 blade and separated from the spinous process. After exposing the articular processes, a pneumatic 1 mm diamond burr was used to decorticate the articular processes. Mice were randomized into 4 different experimental groups: decortication only (n = 5), MSC suspension/gelatin sponge (n = 5), MSC spheroids/gelatin sponge (3D-undiff group) (n = 7), and MSC spheroids with osteogenic induction/gelatin sponge (3D-osteo group) (n = 7). All animals were euthanized by carbon monoxide inhalation 6 weeks after implantation, and their spines were excised for evaluation.

Manual Assessment of Spinal Fusion

Harvested spinal segments were manually tested for intersegmental movement between the L5 and L6 vertebrae of each lumbar vertebra by 2 independent blinded observers. All lumbar vertebrae were scored on a scale of 0-2, with "0" indicating detectable movement between bilateral segments, "1" indicating no movement between segments unilaterally, and "2" indicating no movement between bilateral segments. An average fusion score ≥ 1 was considered successful fusion. The fusion rate was calculated as

$$\text{Fusion rate}\,(\%) = \frac{N_s - N_o}{N_s} \times 100$$

where N_s represents the total number of specimens tested in each group and N_o represents the number of specimens without fusion.

Biomechanical Testing

The biomechanical force of the implanted L5–L6 segment was assessed by applying a downward force perpendicular to the longitudinal axis of the mouse spine. Accordingly, the L5–L6 segments of each specimen were analyzed through a 3-point bending test using an Instron testing machine (H50KT; Instron, MA) to compare the bending stiffness between the following 4 groups: (1) decortication-only group, (2) MSC suspension/gelatin sponge implanted group, (3) MSC spheroids/gelatin sponge treated group, and (4) MSC spheroids with osteogenic induction/gelatin sponge implanted group. Both ends of the L5–L6 segment were positioned with the ventral side positioned down at 2 points. A compressive force was then applied to the dorsal surface of the longitudinal vertebrae through the rod steel of the load cell. 3-point bending tests were performed at a distance of 19 mm between the supports and a head speed of 50 mm/minute. The load–deflection curve of each specimen was obtained from each group, and the compressive force of each displacement was statistically compared.

Micro-computed Tomography

The harvested spinal segments were fixed in 4% paraformaldehyde (PFA) for 1 day until the high-resolution micro-CT examination. All excised tissues were scanned using a Skyscan 1173 micro-CT machine (SkyScan, Kontich, Belgium) with the following settings: X-ray energy 40 keV and 250 μA and exposure time of 520 ms, 18 μm voxel size. For bone histomorphometry, the newly formed bone was isolated from the native bone via a manually drawn volume of

interest (VOI). CT-Analyzer 3D data analysis software was used to analyze the VOI, between the L5 and L5 articular process. To assess new bone formation in fusion mass, the percentage of bone volume (BV) with respect to tissue volume (bone and soft tissue, TV) (BV/TV, %), bone mineral density (BMD, g/cm^3), trabecular thickness (mm), and trabecular number (1/mm) were analyzed.

Hematoxylin-Eosin and Masson's Trichrome Staining

After micro-CT scanning, the spine samples were decalcified using decalcification solution (National Diagnostics, Atlanta, GA), dehydrated with ethanol and xylene, and embedded in paraffin. Cross-sections (5 μm thick) were obtained using a microtome (Leica RM2255; Leica, Berlin, Germany). The sections were stained with hematoxylin and eosin (Sigma) and Masson's trichrome (Sigma).

Immunohistochemistry and Immunofluorescence

For immunohistochemistry and immunofluorescence, the sections were incubated with primary antibodies against osteocalcin (1:3200; Santa Cruz Biotechnology, Dallas, TX, USA), CD-31 (1:200; Abcam, ab119339; Cambridge, MA, USA), and osteopontin (1:200; Abcam, ab8448) for 24 h at 4 °C. After 24 h, the sections were washed with Dulbecco's PBS(DPBS) and incubated with the following secondary antibodies: DISCOVERY UltraMap anti-Rb HRP (Roche Diagnostics Ltd., Basel, Switzerland) and goat anti-rabbit Alexa Fluor 488 (Invitrogen; A11034; 1:200) at room temperature for 1 h. After washing with DPBS, the sections were stained with 4,6-diamidino-2-phenylindole (DAPI) (1:500, Abcam) for 10 minutes. The sections were then mounted and examined using a fluorescence microscope (Zeiss Axioscan Z1, Germany).

Statistical Analysis

The results were presented as means ± SD. All statistical analyses were carried out using the NCSS 10 software program (2015. Kaysville, Utah, USA). One-way analysis of variance (ANOVA) with the Tukey's *post hoc* test was used. Iteration numbers of each experiment could be found in the corresponding figure captions. *, $^{\#}P < .05$; **, $^{\#\#}P < .01$, and ***$P < .001$ were used to indicate significance.

Results

Mass-Production of MSC-Spheroids With Defined Specification

Mass production of MSC spheroids was efficiently achieved by using a GMP-applicable microwell array system. 1 × 10^6 of MSCs initially seeded onto each well of the 6-well plate system could be entirely formed as 2400 of MSC spheroids, while the size and cell number of each spheroid were precisely controlled (~417 cells/spheroid each of which was sized by ~100-μm in diameter, as shown in Fig. 1A and 1B). While the MSC spheroids were cultured for 7 days in either MSC growth medium or osteogenic medium, the sizes and cell numbers were maintained as initially regulated, which were in agreement with the results of earlier studies on MSC spheroids cultured using the FBS-containing medium (Fig. 1A, 1B, and 1C).[31] The results of live and dead assays confirmed that over 90% of the cells in the spheroids of both the 3D-osteo and 3D-undiff groups were viable during 7 days of culture period (Fig. 1D and 1E). This live and dead assay revealed that over 90% of the cellular viability corresponded to the results obtained from a conventional trypan blue viability testing method using single-cell dissociated MSC spheroids (Supplementary Fig. S1). Our flow cytometric analyses for MSC-marker presentation in the MSC-spheroids demonstrated that over 95% of the cells of the 3D-undiff group on day 7 expressed CD44 and CD73, which are positive human MSC-markers, and are similar to the degree with MSCs cultured on the 2D culture plate for 7 days.[22] Contrarily, the 3D-osteo group on day 7 expressed them in significantly lower levels, namely 86.7% and 43.4%, respectively, which indicated that osteogenic differentiation was triggered by 7 days of treatment with the osteogenic medium. In terms of negative MSC-marker expression, such as CD45 and CD34, all groups showed negative results lower than 2% of the expression (Fig. 1F).

Osteogenic Differentiation of Mass-Produced MSC-Spheroids

Mass-produced MSC spheroids were further cultured in osteogenic medium until day 15, and their efficacy in osteogenic differentiation was evaluated by qPCR analyses of the expression of osteogenic genes, such as bone morphogenic protein-2 (BMP2), collagen type I (COL1), runt-related transcription factor-2 (RUNX2), osterix (OSX), alkaline phosphatase (ALP), and osteocalcin (OCN) (Supplementary Figure S2A and S2B). Osteogenic medium successfully induced osteogenic differentiation in both 2D- and 3D-cultured groups in this study. Significantly higher levels of ALP and OSX were found in the 3D-osteo group on days 7 and 15, respectively (compared with those in the 3D-undiff group). The expression of the COL1 gene tended to be higher in the osteogenic medium-treated groups of both 2D and 3D, while all experimental groups showed remarkably high levels of COL1 gene expression (average COL1 gene Ct values of all groups were below 17, while the average Ct values of the house-keeping genes were approximately 18; data not shown). In the comparisons between 2D- and 3D-cultured groups, most of the osteogenic genes, such as BMP2, RUNX2, OSX, and ALP, appeared to be highly upregulated in the 3D-cultured group during the culture period, a result that is in agreement with the results of earlier studies,[25] wherein the expression of the BMP2 gene was significantly upregulated in the 3D-cultured groups by more than several hundredfold compared with that in the 2D-cultured groups. The expression of the OCN gene in the 3D-cultured groups tended to increase with the culture time and was upregulated by the osteogenic medium until day 15 of treatment. However, no significant difference was found among the experimental groups.

Along with our qPCR results, it has been frequently reported that the formation of MSC spheroids enhances the osteogenic differentiation capacity of MSCs.[24-29] Therefore, the osteogenically differentiated MSCs cultured on 2D was excluded in the following investigations since the purpose of our study was to compare between undifferentiated and osteogenically differentiated MSC spheroids regarding therapeutic efficacy in spinal fusion. While MSC spheroids were cultured over 7 days of culture period, some markers of osteogenic differentiation were spontaneously expressed even in the MSC growth medium without osteogenic supplements although MSC markers tended to be maintained. Thus, to maintain the naïve MSC's characteristics in the MSC spheroids, we adopted 4 days of culture period for the 3D-undiff group, whereas 7 days of osteogenic culture period was chosen for the 3D-osteo group in the further analyses that demonstrated successful triggering of osteogenic lineage transition of MSCs.

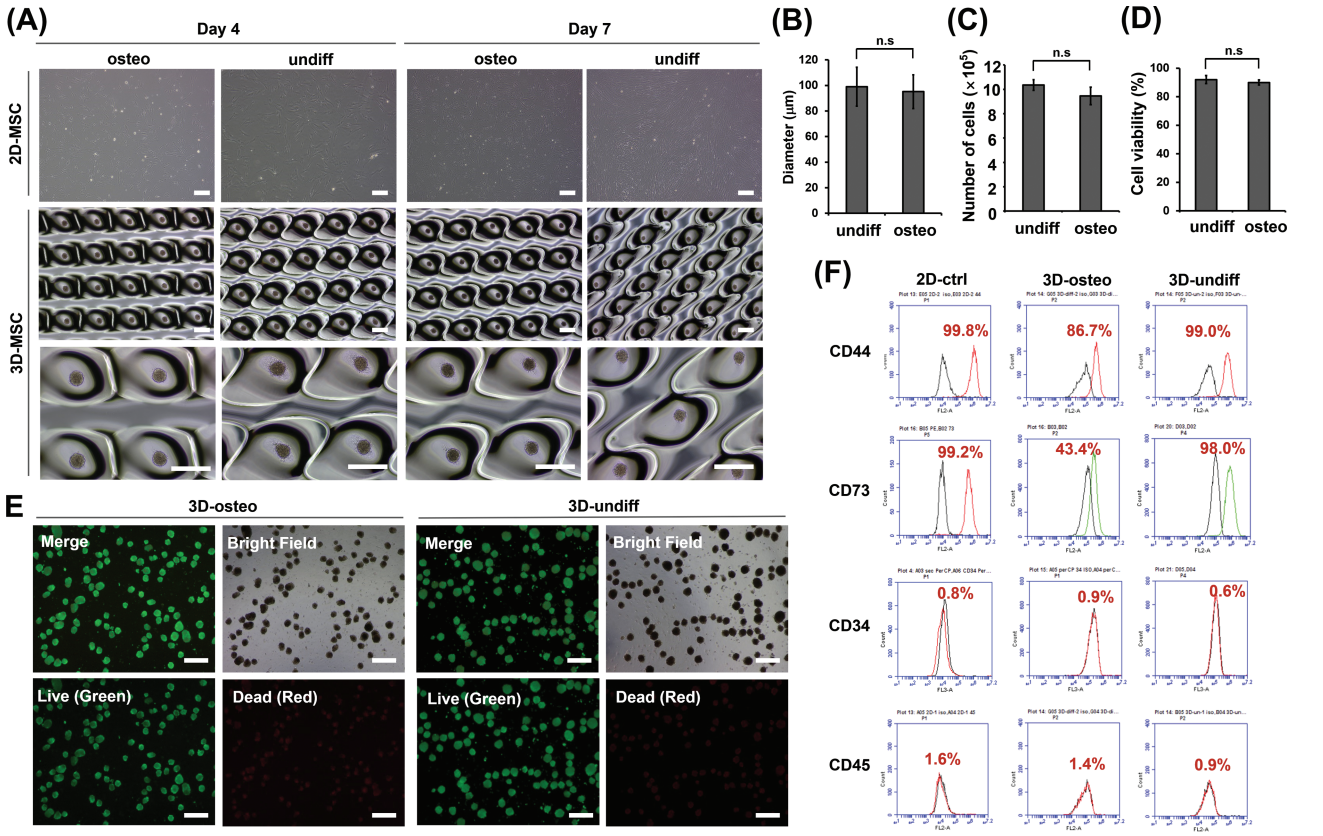

Figure 1. Mass-produced MSC-spheroids. (**A**) Representative images of standard 2D cultured MSC and MSCspheroids formed in the microwell array. 2D- and 3D-MSCs were cultured in growth medium and osteogenic medium. The scale bars indicate 300 μm. Bar plots depicting (B) average of spheroid diameter on day 7. (**C**) Cell numbers of MSC-spheroids was determined on day 7 using a DNA quantification method. The total cell numbers of MSC-spheroids in the single well of the 6-well plate were not increased during the culture period. (**D**) Cell viabilities of the 3D-undiff and 3D-osteo groups on day 7. The quantification data from B to D are expressed as the mean ± SD ($n = 5$). Statistical analyses were performed using a Student's *t* test (ns, not significant). (**E**) Representative images of live and dead assay after calcein-AM and ethidium homodimer-1 staining on day 7 ($n = 5$). The scale bars indicate 500 μm. Graphs illustrating the results of (**F**), flow cytometric analysis for the phenotyping of MSC-spheroids on day 7. Single cells derived from spheroids were immunostained with MSC positive (CD44 and CD73) and negative markers (CD34 and CD45) to confirm cell characterization ($n = 3$).

Accordingly, MSCs cultured on the 2D culture plate for 3 days were taken as the 2D-ctrl group henceforward, which assured the minimized degree of possible spontaneous differentiation.

Protein Expression Profiling of MSC Spheroids Using LC–MS Analysis Supported by Bioinformatics

At the outset, the LC–MS analysis provided quantitative expression profiles of 3606-3782 proteins retained in each of the 2D-ctrl, 3D-osteo, and 3D-undiff groups with relative abundance levels (Fig. 2A). To focus on the proteins of interest, massive protein expression profile data were filtered using bioinformatics. Accordingly, a web-based big data platform for gene ontology and annotation (EBI QuickGO), and text matching algorithm were used to sort out proteins relevant to the bone regeneration mechanism. GO terms with keywords "osteogenesis", "osteoblast", "ossification", and "angiogenesis" were used (Supplementary Table S1). Abundance levels of the extracted proteins were normalized and compared based on log2-transformed mean values to present the overall fold changes of the protein abundance levels in the 2D-ctrl, 3D-osteo, and 3D-undiff groups. Data were selectively presented as angiogenesis-related, both angiogenesis- and osteogenesis-related, and osteogenesis-related proteins by heatmap diagrams (Fig. 2B, 2C, and 2D, respectively). Generally, the 2D-ctrl and 3D-undiff groups displayed more upregulated angiogenic proteins compared with the 3D-osteo group, while the proteins highly expressed in each group were distinguishable (Fig. 2B). In terms of the proteins related to both angiogenesis and osteogenesis, the 3D-undiff group showed higher upregulation in greater numbers of proteins than the other groups (Fig. 2C). In terms of osteogenesis, all groups showed highly upregulated protein expression in different proteins (Fig. 2D).

Analyses of Protein Expressions with Significant Differences

From the heatmap diagrams, the proteins with significant differences ($P < .05$) in the abundance levels compared with those of other groups were separately organized as fold-change charts along with corresponding balloon plots that depict the absolute abundance level of each protein (Fig. 3). Angiogenesis-inducing factors such as fibroblast growth factor-2 (FGF2) were expressed at significantly higher levels in the 2D-ctrl group than in the 3D-cultured groups (both the 3D-osteo and 3D-undiff groups).[33,34] Simultaneously, thrombostin-1 (THBS1) reported as antiangiogenic factor

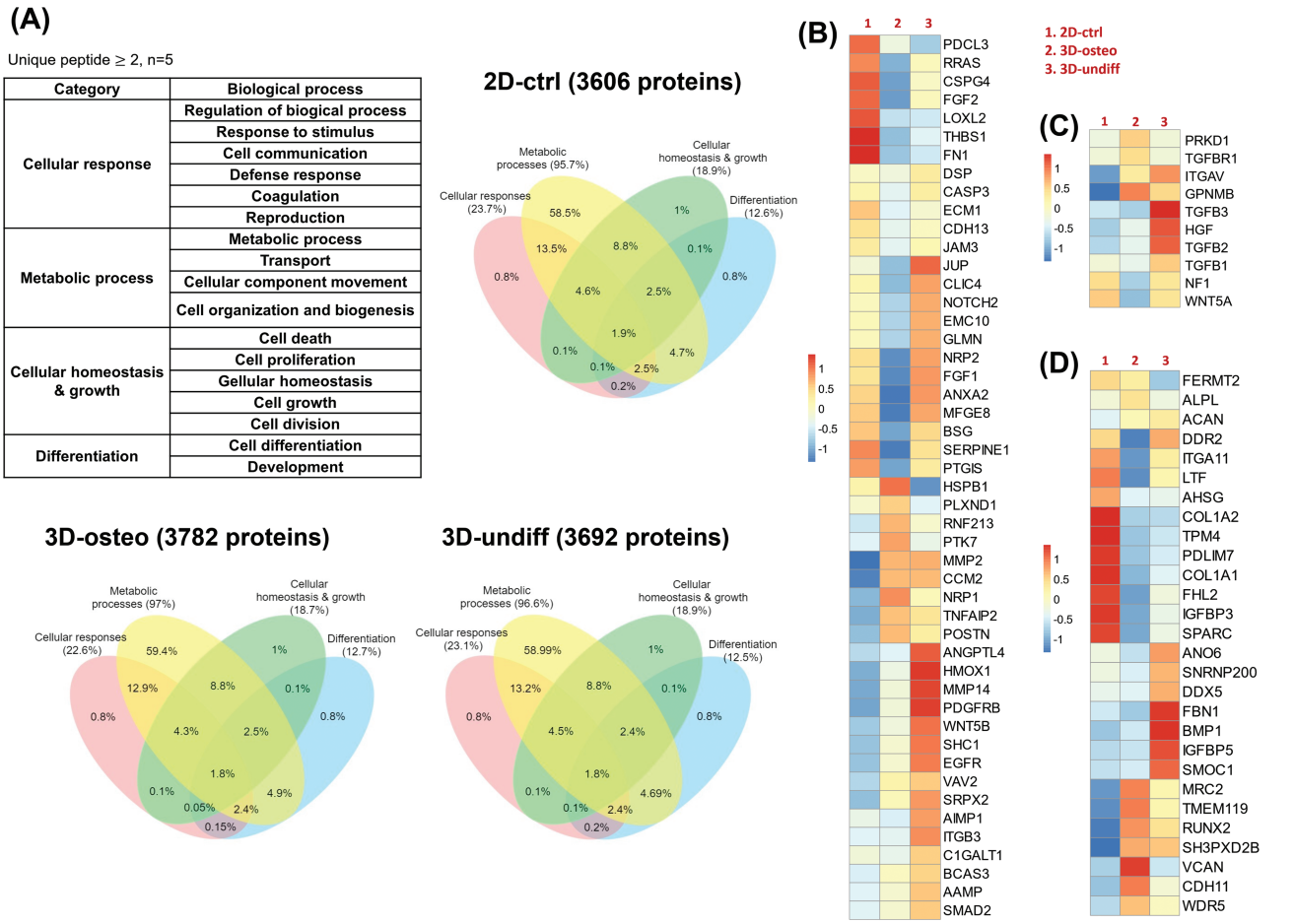

Figure 2. Protein profiling of MSC-spheroids analyzed through LC–MS (n = 5) and subsequent data-filtration based on the bone regeneration mechanism. (**A**) Initial data-base of protein expressions was obtained with detected unique peptides whose numbers were more than 2. Proteins expressed in all groups were categorized according to the biological process and presented using Venn diagrams. Among them, proteins related to (**B**), angiogenic, (**C**), both angiogenic and osteogenic, and (**D**), osteogenic processes were filtered by using a web-based big data platform and presented by heat map diagrams. Heat map colors are assigned according to an abundance level relative scale, from –1 to 1.

that inhibits the proangiogenic actions of FGF2 was concurrently expressed at the highest level in the 2D-ctrl group among all groups.[35,36] Additionally, chondroitin sulfate proteoglycan-4 (CSPG4) and lysyl oxide homolog-2 (LOXL2) that are related to endothelial cell migration and proliferation in the blood vessel basement membrane were also expressed at significantly higher levels in the 2D-ctrl group than in the 3D-cultured groups.[37-39] The 3D-cultured groups showed significantly higher expressions than the 2D-ctrl group in different angiogenesis-related proteins, such as platelet-derived growth factor receptor beta (PDGFRB), heme oxygenase-1 (HMOX1), matrix metalloproteinase-2 (MMP2), and MMP14 that contributes to angiogenesis as a key effecter of vascular endothelial growth factor (VEGF) and MMP2 activation.[40-44] PDGFRB, HMOX1, and MMP14 were expressed at the highest levels in the 3D-undiff group. Simultaneously, other proteins related to angiogenic signals, such as WNT family members 5A and 5B (WNT5A and WNT5B), epidermal growth factor receptor (EGFR), and integrin beta-3 (ITGB3) were also highly upregulated in the 3D-undiff group.[45-48] The 3D-osteo group appeared to show a different pattern with respect to protein expression as it expressed fewer soluble bioactive molecules than the other groups. Heat shock protein beta-1 (HSPB1) was expressed at the highest level in the 3D-osteo group among all groups, which is known to regulate angiogenic balance by means of negative feedback to the angiogenic promotion activity of VEGF.[49] Contrastingly, the 3D-undiff group showed significantly higher levels of upregulation of most proteins known to play crucial roles in inducing both angiogenesis and osteogenesis (compared to other groups). The 3D-undiff group showed significantly higher expression levels of the key growth factors involved in both angiogenesis and osteogenesis, such as transforming growth factor beta-2 and -3 (TGFB2 and TGFB3), and hepatocyte growth factor (HGF).[50-54] TGFB1 was also found to be upregulated in the 3D-undiff group (with a statistical difference compared to the 3D-osteo group). Summarily, the 3D-cultured groups displayed significantly higher levels of expression of some proteins related to both angiogenesis and osteogenesis (than the 2D-ctrl group), such as transmembrane glycoprotein NMB (GPNMB, also known as osteoactivin) that promotes osteoblast differentiation as well as endothelial cell migration and proliferation, thus supporting bone regeneration,[55-57] and integrin alpha-V (ITGAV) known to play a role in the regulation of angiogenesis and osteogenesis through introducing the pathways of FGFs and insulin like growth factors (IGFs).[48,58] In terms of osteogenesis promotion as well as osteogenic induction, the 2D-ctrl group

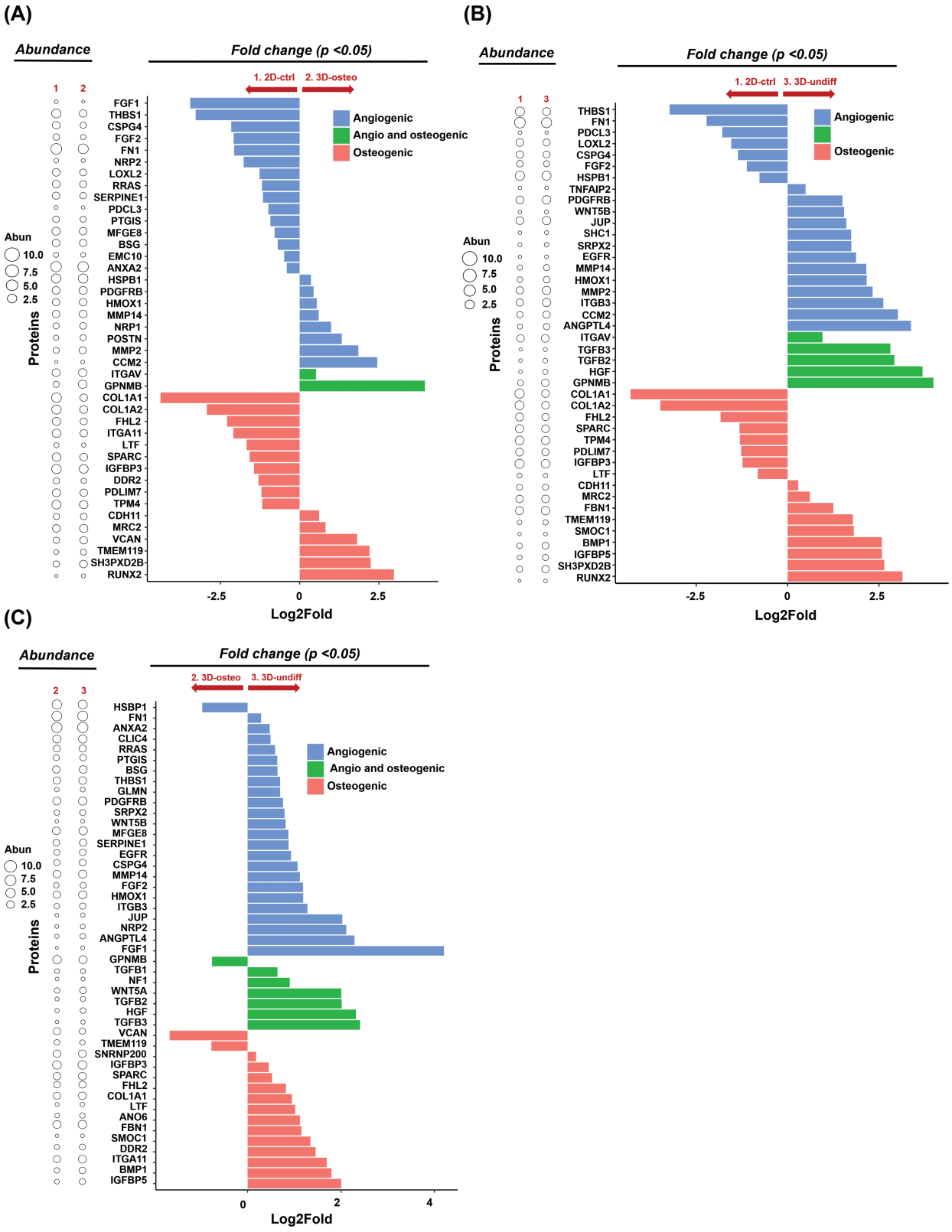

Figure 3. Charts depicting proteins with statistical significance in the abundance levels. Differential expression of proteins with significant differences ($P < .05$) between (**A**), the 2D-ctrl and 3D-osteo groups, (**B**), the 2D-ctrl and 3D-undiff groups, and (**C**), the 3D-osteo and 3D-undiff groups were presented by log2 foldchange chart. Statistical analyses were performed using a Student's *t* test. The abundance levels of each protein were visualized using balloon plot. Proteins related to angiogenic, both angiogenic and osteogenic, and osteogenic processes are depicted with different colors (blue, green, and light red, respectively) based on the indicated bone regeneration mechanism.

showed significantly higher upregulations of the bone matrix proteins than other groups, such as collagen type I alpha-1 and -2 (COL1A1 and COL1A2), together with secreted protein acidic and rich in cysteine (SPARC/osteonectin) that is bound to collagen type I to nucleate mineral phase deposition.[59,60] Proteins related to osteogenic differentiation signals such as 4 and a half LIM domains protein-2 (FHL2), lactotransferrin (LTF), and PDZ and LIM domain protein 7 (PDLIM7/LMP1) were also highly upregulated in the 2D-ctrl group.[61-63] GPNMB, the 3D-osteo group, showed the highest upregulations in versican (VCAN), one of the important bone matricellular proteins that regulate osteogenic differentiation of MSCs,[64] and transmembrane protein 119 (TMEM119) that regulates the BMP-RUNX2 pathway to promote the differentiation of osteoblast and matrix mineralization.[65] Generally, both the 3D-osteo and 3D-undiff groups showed significantly higher expression than the 2D-ctrl group in TMEM119, SH3, and PX domain-containing protein 2B (SH3PXD2B), and RUNX2, the most central transcription factor for osteogenic differentiation.[66-68] In the 3D-undiff group, several important regulators for osteogenic differentiation, matrix mineralization, and bone remodeling were found to be upregulated with statistical difference, which include fibrillin1 (FBN1), SPARC-related modular calcium-binding protein 1 (SMOC1), BMP1, and IGF-binding protein-5 (IGFBP5).[69-72]

Numbers of MSC-specific proteins were also investigated by the LC–MS analysis such as CD44, CD73, THY1 (CD90), ENG (CD105), ANPEP (CD13), ITGB1 (CD29), TFRC (CD71), ALCAM (CD166), MME (CD10), MCAM (CD146), SDC2 (CD362), CD9, VIM, and NES (Supplementary Table S2 and Fig. S3). The results showed that significantly higher expressions of the MSC-specific proteins were found in the 2D-ctrl and 3D-undiff groups compared with the 3D-osteo group, while showing some variances in each protein expression between them.

The above-stated protein expression profile of each group is summarized and depicted with the predictable contributions to bone regeneration after transplantation, which include neoangiogenesis and osteogenic induction in host tissues as well as transplanted angiogenic or osteogenic differentiation MSCs shown in Fig. 4. Based on the physical, biochemical, and therapeutic properties of MSC spheroids obtained in this study, possible quality control (QC) standards and assay methods were suggested (Supplementary Table S3 and Fig. S4).

Mouse Spinal Fusion Model

Manual Fusion Test

Six weeks after implantation, the fusion rate was measured by manual palpation. Fusion rates were significantly higher in mice implanted with the 3D-undiff group (75%) and 3D-osteo group (62.5%) than in mice implanted with the 2D-ctrl group (42.8%) and those that underwent decortication alone (0%) (Fig. 5A).

Biomechanical Evaluation

To evaluate the biomechanical properties of the newly formed bone in a mouse posterolateral spinal fusion model, L5–L6 specimens were isolated from each mouse 6 weeks after implantation to perform a 3-point bending test. There was no significant difference in the initial slopes among groups (G1: decortication only, G2: 2D-ctrl in gelatin sponge, G3: 3D-undiff in gelatin sponge, and G4: 3D-osteo in gelatin sponge). However, when the displacement was increased to more than 6 mm, both G3 and G4 showed a significant increase in strength compared with that in the decortication only group. There was no significant difference in the biomechanical properties of the newly formed bone in both G3 and G4 (Fig. 5B).

Micro-computed Tomography Analysis

New bone formation was determined using micro-CT analysis 6 weeks after implantation. Based on micro-CT images, new bone formation was evaluated by measuring parameters such as the percentage of bone volume (BV) with respect to tissue volume (TV) (BV/TV, %), BMD, trabecular thickness, and trabecular number (Fig. 5C). BV/TV (%), BMD (g/cm^3), trabecular thickness (mm), and trabecular number (1/mm) were found to be significantly higher in 3D-undiff (G3) and 3D-osteo (G4) groups than those in decortication only (G1) and 2D-ctrl (G2) group. New bone formation was not detected in decortication only (G1) group. MSC suspension/gelatin sponge-treated group (G2) showed slightly increased new bone mass compared with decortication only group, although no significant difference was found. A large volume of newly formed bone was observed in groups 3D-undiff (G3) and 3D-osteo (G4) groups. Particularly, 3D-undiff (G3) group showed clear evidence of significantly increased BV/TV, BMD, trabecular thickness, and trabecular number compared with the other groups (Fig. 5C).

Histological Analysis

At the end of the 6-week period, we euthanized the animals to histologically explore the bone regeneration efficacy of all groups. Spinal samples from each group were decalcified and analyzed by hematoxylin and eosin (H&E), and Masson's trichrome (MT) staining (Fig. 6). Histological analyses of HE and MT staining demonstrated that the amount and area density of new bone formations were significantly increased in both 3D-undiff (G3) and 3D-osteo (G4) groups compared with decortication only (G1) and 2D-ctrl (G2) groups, while no significant difference was found in 3D-undiff (G3) and 3D-osteo (G4) groups. Immunohistochemical analysis of osteocalcin and immunofluorescent analysis of osteopontin confirmed the induction of endochondral bone formation in the implanted sites as bone remodeling markers (Figs. 6 and 7). In the results of the average immunoreactivity of osteocalcin and osteopontin, 3D-undiff (G3) and 3D-osteo (G4) groups demonstrated significantly higher expression levels of both osteocalcin and osteopontin compared with decortication only (G1) and 2D-ctrl (G2) groups, while 3D-undiff (G3) and 3D-osteo (G4) groups were not significantly different. Immunofluorescent analysis for CD31, a common endothelial cell marker, was also performed to observe the neoangiogenic efficacy after implantation in all groups (Fig. 7). Significantly higher expression of CD31 was observed in 3D-undiff (G3) and 3D-osteo (G4) groups than in decortication only (G1) and 2D-ctrl (G2) groups, which suggested that exceedingly activated angiogenesis occurs in the implanted sites of the 3D-undiff and 3D-osteo groups.

Discussion

Spinal fusion is a surgical method that connects 2 adjacent vertebrae when there is a vertebral fracture or spinal stenosis

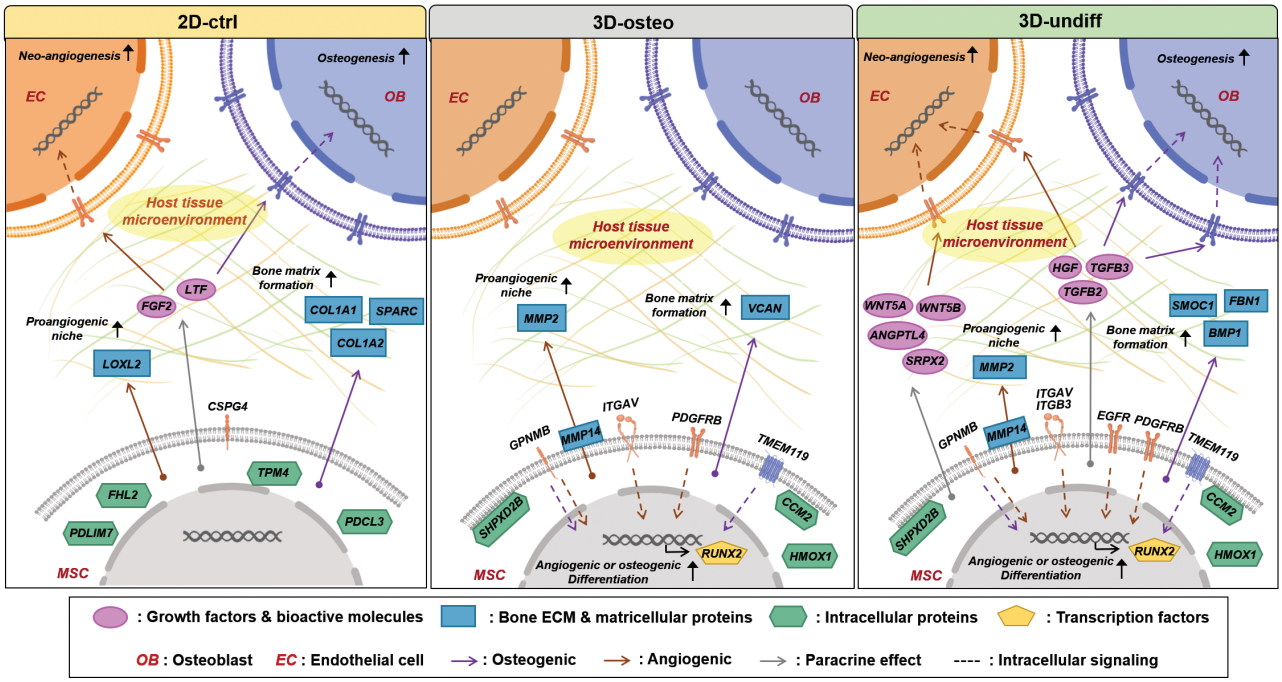

Figure 4. Schematic illustrating the description of the predictable contributions of each group to bone regeneration after transplantation, including neo-angiogenesis and osteogenic induction in host tissues as well as transplanted angiogenic or osteogenic differentiation of MSCs.

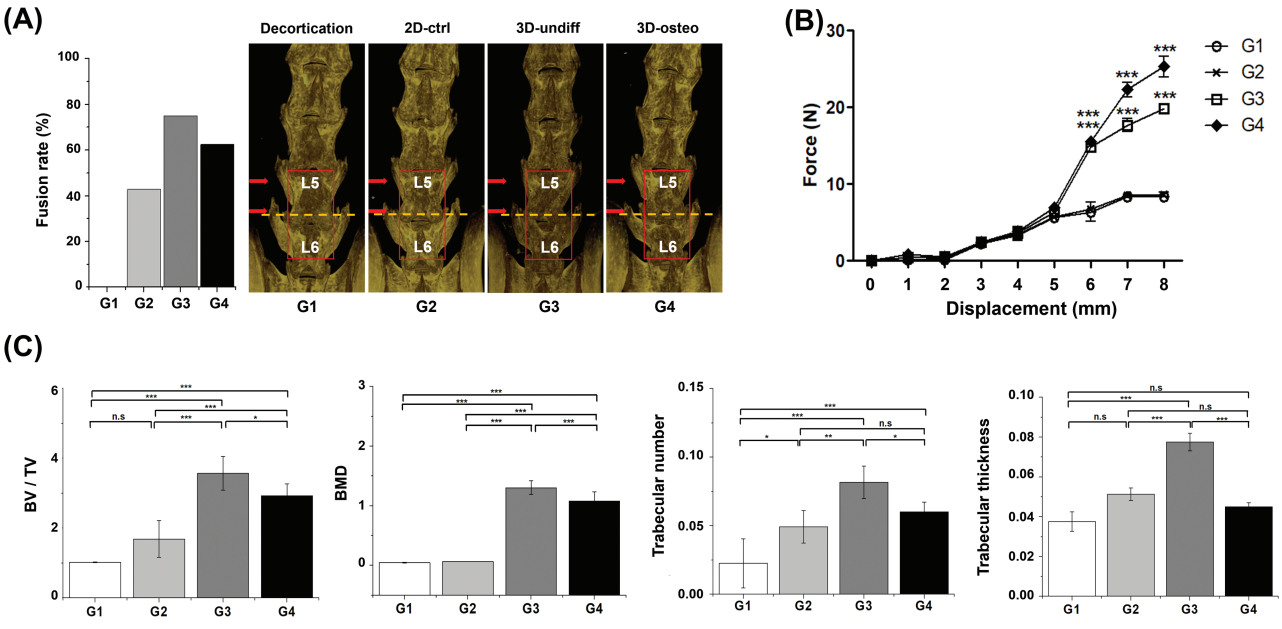

Figure 5. In vivo spinal fusion results at 6 weeks post-implantation. (**A**) Representative 3D micro-CT images of the L5-L6 fusion mass. (**B**) Line plot depicting biomechanical assessment of fusion mass by three-point bending test. Force–displacement curves of fusion mass for each group. (**C**) Bar plots illustrating the bone histomorphometric analysis of percent bone volume (BV/TV, %), bone mineral density (BMD, g/cm^3), trabecular thickness (mm), and trabecular number (1/mm). G1: decortication only, G2: 2D-ctrl in gelatin sponge, G3: 3D-undiff in gelatin sponge, and G4: 3D-osteo in gelatin sponge. Data are presented as mean ± SD (n = 5-7; *P < .05; **P < .01; ***P < .001; ns, not significant) and analyzed by one-way ANOVA followed by Tukey's post hoc test.

with severe nerve compression. The frequency of spinal fusion surgery is rapidly increasing due to an increase in the elderly population and an increase in accident.[1-4] A wide variety of bone substitutes are used clinically to support spinal fusion. Despite the recent development of various bone substitutes, there are still many reports of pseudarthrosis (nonunion, fusion failure) that cause severe back pain after the surgery, which places heavy demands on the investigations using stem cell-based medicinal products to address the current limitations.[1,3,10-15] Therefore, a preclinical study of the application of MSC spheroids as a new bone tissue substitute, either undifferentiated or osteogenically differentiated, to a mouse spinal fusion model was conducted and compared with MSCs conventionally cultured on a monolayer. For this preclinical study,

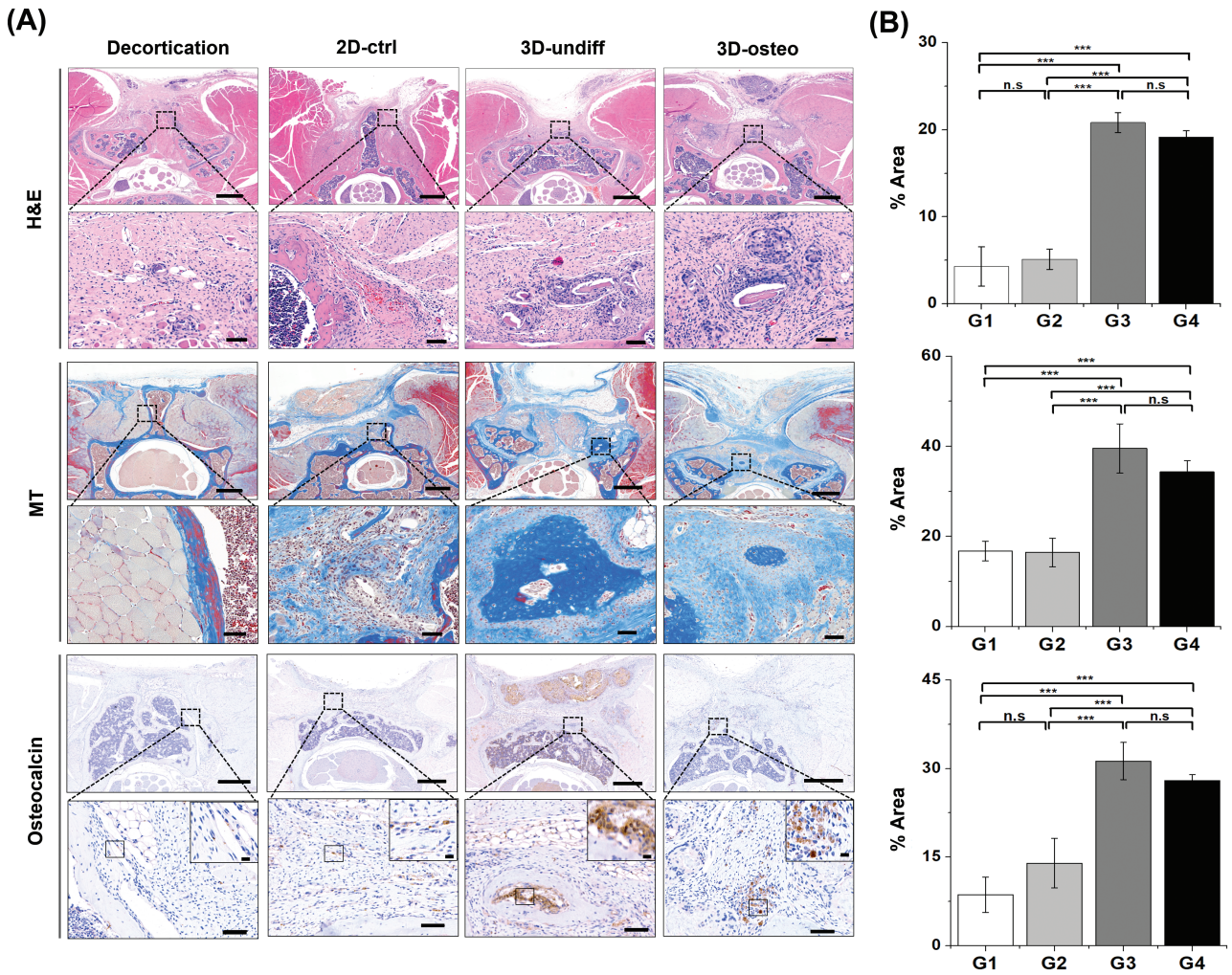

Figure 6. Histological and immunohistochemical analyses at 6 weeks post-implantation. (**A**) Image showing cross-sections of spinal fusion stained with hematoxylin and eosin (H&E) and Masson's trichrome staining (MT), and immuno-staining images of osteocalcin. The scale bars of H&E, MT, and osteocalcin indicate 500 μm at low magnification (upper panels) and 50 μm at high magnification (lower panels), respectively. The scale bars of inset images on the osteocalcin expression analysis indicate 10 μm. (**B**) Bar plots depicting quantitative analyses of the amount and area density of new bone formations detected by H&E and MT staining and the average immunoreactivity of osteocalcin detected by the positive area of anti-osteocalcin. Data are presented as mean ± SD ($n = 7$; *$P < .05$; **$P < .01$; ***$P < .001$; n.s., not significant) and analyzed by one-way ANOVA followed by Tukey's post hoc test.

we developed an efficient method for the secure delivery of MSC spheroids to the decorticated sites on the lumbar spine by utilizing gelatin sponge clinically approved and used for hemostatic dressing, which possesses the ability to finely attach to the wounded region. Owing to the high porosity and water-loving characteristics of the gelatin sponge, a droplet containing MSC spheroids would be immediately absorbed so that the MSC spheroids could be steadied to successfully assure the engraftment of MSCs after implantation. Based on the results of previous preclinical and clinical studies, it is estimated that immunological responses are regulated by increasing nucleus pulposus cells-like gene expression and improving ECM production when MSCs are injected for treatment in degenerative disc disease, osteoporotic fracture models spinal cord injury models and spine fusion models. Still immune rejection is an issue for allogeneic and xenogeneic cell transplantation as well. Nevertheless, it is known that MSCs have a relatively low immunogenicity due to the low expression rate of MHC Class I and can also be expected to have a therapeutic effect using immunomodulatory effects clinically.[17,73-77] Moreover, the MSCs are immune privileged with immunosuppressive abilities even though the animals were not treated with immunosuppressive drugs using in vivo human MSC xenograft models, suggesting an unrecognized immune-privileged site within the IVD space and the central nervous system. Furthermore, the MSCs isolated from bone marrow, adipose tissue, and Warton jelly have the proliferative potential, the weak expression of MHC II genes, and the weak expression of the immune-related genes including TLR4, TLR3, JAG1, NOTCH2, and NOTCH3.[73-77] The much higher efficacy of the 3D-cultured groups was observed in our mouse spinal fusion model than in the 2D-ctrl group, a finding that is surprisingly consistent with the growing evidence supporting the therapeutic benefits of spheroid cultures for stem cells.[24,25] Our bone histomorphometric analyses revealed that both the 3D-cultured groups were well integrated into the decorticated sites of the lumbar spine after implantation and efficiently supported spinal fusion, as proven by the mechanical tensile strength evaluation of the fused spinal mass representing robust mechanical stability. As shown in

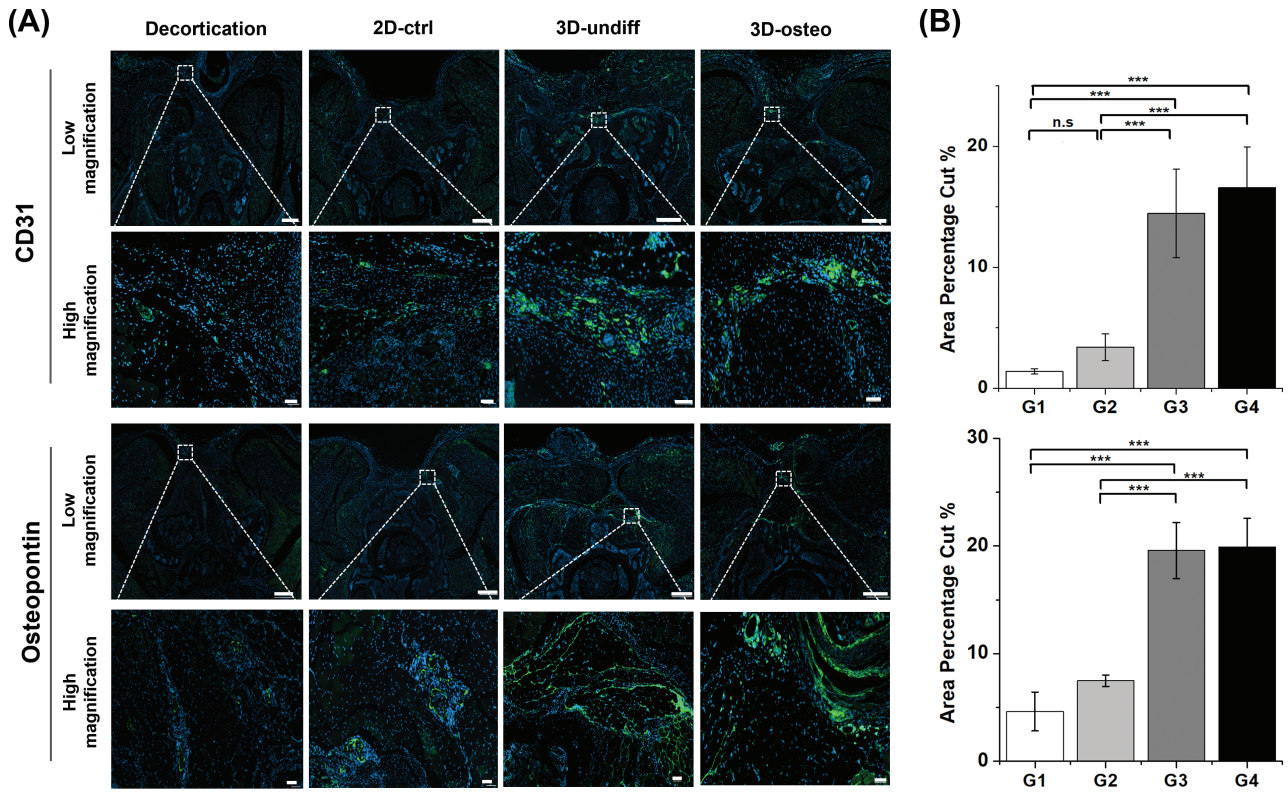

Figure 7. Immunofluorescent analyses at 6 weeks post-implantation. (**A**) Image depicting cross-sections of spinal fusion region stained with anti-CD31 and anti-osteopontin. The scale bars of CD31 and osteopontin indicate 500 μm at low magnification (upper panels) and 50 μm at high magnification (lower panels), respectively. (**B**) Bar plots of the quantitative analyses of the average immunoreactivity of anti-CD31 and anti-osteopontin. Data are presented as mean ± SD ($n = 7$; $^{*}P < .05$; $^{**}P < .01$; *** $P < .001$; n.s., not significant) and analyzed by one-way ANOVA followed by Tukey's post hoc test.

our histological and immunohistochemical analyses, the recruitment of osteogenic cells and/or induction of osteogenic differentiation on site may have been triggered by implantation of either the 3D-osteo or 3D-undiff group, which could result in newly synthesized bone matrix and contribute to bone regeneration. Additionally, immunofluorescence analysis of anti-CD31 indicated that neo-angiogenesis was also stimulated by both 3D-cultured groups, which resulted in the formation of a new vascular bed.

As transcriptome data that analyze mRNA expression cannot completely represent the abundance of protein expression, direct measurement of protein activities is essential to understand cellular mechanisms.[78] Accordingly, LC–MS has contributed to the remarkable advancement in analyzing complex biological processes, which enables the identification and quantification of thousands of proteomes extracted from a batch of cultured cells or biopsied tissues. Bioinformatics technologies have rapidly facilitated the spectral data analysis, management, and visualization of the massive proteomic data obtained by LC–MS, along with the implementation of biostatistics.[79] In this study, we used LC–MS methodology and bioinformatic tools to gain a detailed understanding of the changes in the proteome within MSC spheroids in comparison to MSCs cultured on a monolayer. Bone regeneration mechanisms include a variety of cells in the defected bone tissue, such as osteogenic and vasculogenic cells (osteoblasts (OBs) and endothelial cells (ECs), respectively), which are surrounded by osteogenesis- and angiogenesis-inductive signaling factors secreted by themselves.[80] Additionally, bone ECM is reorganized with specifically controlled mechanical and biochemical properties with accumulated matricellular proteins to nucleate mineral deposition, further promote osteogenic differentiation of OBs, and introduce ECs for neo-angiogenesis.[81,82] In view of such bone regeneration mechanisms, we attempted to describe the predictable contributions of 2D-ctrl, 3D-osteo, and 3D-undiff groups to bone regeneration after implantation based on our LC–MS protein profiling data (Fig. 3). Proteomic analyses revealed that multiple soluble proteins were significantly upregulated in the 3D-undiff group, which could act as paracrine effectors for osteogenesis and/or angiogenesis induction in host bone tissues. Among others expressed most significantly in the 3D-undiff group, HGF and TGFBs have often been reported as key growth factors that stimulate osteogenesis as well as angiogenesis.[50-54] Contrastingly, the 3D-osteo group exhibited evidence of differentiation toward a pre-osteogenic lineage as expressing the highest degree of RUNX2 (also shown in our qPCR results), a representative marker for committed osteoprogenitor at the early stage of osteogenesis.[83] VCAN expression was also most highly upregulated in the 3D-osteo group, which is required for the wide-ranging remodeling of the ECM in the early phase of bone formation and accelerates the differentiation of MSCs into osteoblasts.[66] Simultaneously, the 3D-cultured groups commonly expressed transmembrane proteins, including receptors related to the regulation of MSC osteogenic differentiation, matrix mineralization, and angiogenesis induction, such as PDGFRB,[40] GPNMB,[55-57] ITGAV,[48,58] and TMEM119,[65] which may facilitate the induction of immediate cellular responses to the host

tissue microenvironment. Additionally, the proteomic data also indicated that both the 3D-cultured groups could support proangiogenic niche formation by secreting MMP2 and MMP14 to recruit ECs to migrate toward the implanted site,[42-44] thus developing dense vascular beds to deliver sufficient oxygen, nutrients, and hormones, in addition to recruiting circulating OBs and MSCs for accelerating bone regeneration.[84] The proteome information of both the 3D-cultured groups was shown to be distinguished while having shared protein expression patterns. Therefore, the osteoprogenitor-spheroids of the 3D-osteo group and undifferentiated MSC spheroids of the 3D-undiff groups may have in some respects contributed to bone regeneration in different paths but resulted in similar therapeutic outcomes after implantation. As reported by many earlier studies, bone regeneration processes are regulated by synergistic association and elaborate interplay among OBs, ECs, and MSCs as sharing extensive paracrine communication.[85-87] Concentrated angiogenic signaling crosstalk between MSCs and ECs or OBs and ECs could initiate migration of ECs to stimulate neo-angiogenesis and the resulting outgrowth of ECs is combined with the host vascular tissues.[88,89] During this process, MSCs and OBs are more attracted to the newly formed vascular beds and establish a close physical proximity to ECs with enhanced expression of osteoinductive factors, which in turn trigger osteogenic differentiation on site and contribute to bone matrix synthesis.[90,91] Hence, based on our biomolecular comprehension and in vivo efficacy results of the 3D-cultured groups, we speculate that such intimate signaling crosstalk between MSCs and ECs or OBs and ECs in bone regeneration could be reproduced by our 3D-undiff or 3D-osteo group, respectively, although relevant physiological investigations presented in this study are limited to fully demonstrate the situ multifactorial cellular interplay which may occur after their implantation. Although both the 3D-osteo and 3D-undiff groups showed similar degrees of bone regeneration efficacy and spinal fusion rate in our animal study, the 3D-osteo group has significant disadvantages for use in clinical settings. This is because the osteogenesis-induction process in the 3D-osteo group can cause methodological complexity with laborious steps of medium exchange during the extended culture period of 7 or 15 days, which requires highly trained culture experts in the microwell array–based MSC spheroid culture system. The increased degree of manipulation in manufacturing the biological products will lead to poor control of the key intermediates in the production processes, so that relevant quality assurance tasks for the follow-up of all deviations from the defined specifications of the final product will become more intense and thus represent a financial challenge due to the increased QC costs.[92,93] Additionally, the use of additional reagents for osteogenic supplements could also lead to substantially extra costs in large-scale manufacturing for commercial purposes and introduce the intricacies to convince the absence of adventitiously introduced contaminants that may affect the properties or stability of the final product.[94,95] Contrastingly, the 3D-undiff group was maintained undifferentiated in the conventional MSC growth medium that was casually used for previously licensed MSC therapies.[96] Additionally, the MSC spheroids in the 3D-undiff group could be stably mass-produced in our microwell array culture system without any disturbance during 4 days of a relatively short culture period, in which the laborious culture steps of medium exchange are not required. This would lead to the ease of preparation for the new standard operating procedure (SOP) as well as detailed specifications for all reagents that satisfy the GMP requirements to ensure consistent and reproducible final product of MSC spheroids. Furthermore, unlike the 3D-osteo group, the 3D-undiff group exhibited elevated levels of MSC markers similar or even higher than the original MSCs, while certain biological activities related to bone regeneration tend to be increased to a greater extent than those in the other groups (Supplementary Fig. S3). This undifferentiated status of our 3D-undiff group could be advantageous in the development of QC standards for MSC spheroid therapy, which could be simplified by following the minimal defining criteria of human MSCs previously established by the International Society for Cell and Gene Therapy (ISCT, www.isctglobal.org),[97] and readily supported by a substantial amount of clinical experience with respect to human MSCs. Therefore, we chose the 3D-undiff group in this study as a suitable candidate for bone tissue substitutes in spinal fusion surgery to reach the earliest clinical translation of MSC spheroids.

Detailed specifications of the physical, biochemical, and therapeutic properties of MSC spheroids were obtained from our preclinical study, with which a framework of the QC standards for MSC spheroids was proposed in this study (Supplementary Table S3), in regard to the identity, purity, viability, and potency within an appropriate limit, range, or distribution, as per the guidelines preliminarily established by global regulatory bodies for licensed MSC drugs.[98,99] The QC standards for the identity, purity, and viability could be suggested with reference to the existing guidelines for MSC therapies. However, the therapeutic activity or intended biological effect is often discriminated depending on the individual product attributes so that the acceptability of potency assay methods and standards should be reviewed on a case-by-case basis.[17,99] In this study, we verified significantly upregulated paracrine factors critical for the induction of osteogenesis and/or angiogenesis, such as HGF, TGFB1, TGFB2, and TGFB3 in the 3D-undiff group, which were suggested as markers for measuring the potency of our final product. We obtained the average content of TGFB1 in 6000 MSC spheroids (2.5×10^6 cells) using a commercialized ELISA kit for TGFB1 to suggest the potency measurement method in this study (Supplementary Fig. S4). Further biological investigations are needed to validate the interrelations of the proposed potency markers in bone regeneration and to characterize relevant mechanisms of action. Microbiological testing, including sterility, adventitious agent, mycoplasma, genomic stability, short tandem repeat assay, and donor eligibility was not discussed in this work, which has been regularly standardized for cell-based therapy and can be externalized by a GMP-accredited laboratory. The safety of the implanted stem cells is also a central consideration in the clinical settings. Although MSC implantation therapy has been shown to be safe in a number of clinical studies,[100] there have been no report addressing the clinical safety of 3D-cultured MSC spheroids. With the objective of clinically employing our undifferentiated MSC spheroids in spinal fusion surgery, Good Laboratory Practice (GLP)-compliant toxicology studies should be conducted by a certified nonclinical contract research organization.

Conclusion

While increasing research evidence promises more powerful therapeutic implementation of 3D-cultured MSC spheroids than MSCs conventionally cultured on a monolayer, there

have been few cases of successful translation into the clinic. The main clinical challenges with MSC spheroid therapies would be present in a series of critical issues in compliance with the current legal requirements regarding the design of a large-scale manufacturing process applicable for GMP, the assurance of standards for QC and safety, and the development of reliable analytical methods to evaluate the final medicinal products.[17] However, a lack of studies published regarding such issues is problematic to reach the clinical translation of MSC spheroids. We believe that our study makes a meaningful contribution to the clinical application of MSC spheroids in spinal fusion surgery as a new bone tissue substitute and further inspiration for the versatile use of MSC spheroids in the biohealth industry.

Acknowledgment

We are thankful to the Korea Centers for Disease Control and Prevention (2018ER610300) and the National Research Foundation of Korea (2020R1A2C4001870 and 2020R1F1A1072695) for the research grants that supported this work.

Funding

None declared.

Conflict of Interest

The authors declared no potential conflicts of interest.

Author Contributions

J.M.C. and I.H.: administrative support, conception and design—review and editing; S.C. and H.C.: collection and assembly of data, data analysis and interpretation, manuscript writing– original draft; H.J.: investigation, methodology, software, data curation; S.Y.K., E.J.R., K.J., and I.B.: data analysis and interpretation; B.J.K.: methodology, project design; S.L.: conception and design.

Data Availability

The data included in this study are available from the corresponding authors upon reasonable request.

Supplementary Material

Supplementary material is available at *Stem Cells Translational Medicine* online.

References

1. Bedair TM, Lee CK, Kim DS, et al. Magnesium hydroxide-incorporated PLGA composite attenuates inflammation and promotes BMP2-induced bone formation in spinal fusion. *J Tissue Eng*. 2020;11:2041731420967591. https://doi.org/10.1177/2041731420967591
2. Hofler RC, Swong K, Martin B, et al. Risk of pseudoarthrosis after spinal fusion: analysis from the healthcare cost and utilization project. *World Neurosurg*. 2018;120:e194-e202. https://doi.org/10.1016/j.wneu.2018.08.026
3. Hwangbo H, Lee H, Roh EJ, et al. Bone tissue engineering via application of a collagen/hydroxyapatite 4D-printed biomimetic scaffold for spinal fusion [in English]. *Appl Phys Rev*. 2021;8(2).
4. Joaquim AF, Lee NJ, Riew KD. Circumferential operations of the cervical spine. *Neurospine*. 2021;18(1):55-66. https://doi.org/10.14245/ns.2040528.264
5. Rihn JA, Kirkpatrick K, Albert TJ. Graft options in posterolateral and posterior interbody lumbar fusion. *Spine (Phila Pa 1976)*. 2010;35(17):1629-1639. https://doi.org/10.1097/BRS.0b013e3181d25803
6. Vaccaro AR, Whang PG, Patel T, et al. The safety and efficacy of OP-1 (rhBMP-7) as a replacement for iliac crest autograft for posterolateral lumbar arthrodesis: minimum 4-year follow-up of a pilot study. *Spine J*. 2008;8(3):457-465. [in English]. https://doi.org/10.1016/j.spinee.2007.03.012
7. Wang W, Yeung KWK. Bone grafts and biomaterials substitutes for bone defect repair: a review. *Bioact Mater*. 2017;2(4):224-247. https://doi.org/10.1016/j.bioactmat.2017.05.007
8. Chang HK, Huang M, Wu JC, et al. Less opioid consumption with enhanced recovery after surgery Transforaminal Lumbar Interbody Fusion (TLIF): a comparison to standard minimally-invasive TLIF. *Neurospine*. 2020;17(1):228-236. https://doi.org/10.14245/ns.1938422.211
9. Manzur MK, Steinhaus ME, Virk SS, et al. Fusion rate for stand-alone lateral lumbar interbody fusion: a systematic review. *Spine J*. 2020;20(11):1816-1825. https://doi.org/10.1016/j.spinee.2020.06.006
10. Casanova MR, Oliveira C, Fernandes EM, et al. Spatial immobilization of endogenous growth factors to control vascularization in bone tissue engineering. *Biomater Sci*. 2020;8(9):2577-2589. https://doi.org/10.1039/d0bm00087f
11. Duarte RM, Varanda P, Reis RL, et al. Biomaterials and bioactive agents in spinal fusion. *Tissue Eng Part B Rev*. 2017;23(6):540-551. https://doi.org/10.1089/ten.TEB.2017.0072
12. Ho-Shui-Ling A, Bolander J, Rustom LE, et al. Bone regeneration strategies: engineered scaffolds, bioactive molecules and stem cells current stage and future perspectives. *Biomaterials* 2018;180:143-162. https://doi.org/10.1016/j.biomaterials.2018.07.017
13. Jang HJ, Park SB, Bedair TM, et al. Effect of various shaped magnesium hydroxide particles on mechanical and biological properties of poly(lactic-co-glycolic acid) composites. *J Ind Eng Chem*. 2018;59:266-276. [in English].
14. Lin S, Cui L, Chen G, et al. PLGA/beta-TCP composite scaffold incorporating salvianolic acid B promotes bone fusion by angiogenesis and osteogenesis in a rat spinal fusion model. *Biomaterials* 2019;196:109-121. https://doi.org/10.1016/j.biomaterials.2018.04.004
15. Nakajima T, Iizuka H, Tsutsumi S, et al. Evaluation of posterolateral spinal fusion using mesenchymal stem cells. *Spine* 2007;32(22):2432-2436. [in English]. https://doi.org/10.1097/BRS.0b013e3181573924
16. Heo JS, Choi Y, Kim HS, et al. Comparison of molecular profiles of human mesenchymal stem cells derived from bone marrow, umbilical cord blood, placenta and adipose tissue. *Int J Mol Med*. 2016;37(1):115-125. https://doi.org/10.3892/ijmm.2015.2413
17. Guadix JA, Lopez-Beas J, Clares B, et al. Principal criteria for evaluating the quality, safety and efficacy of hMSC-based products in clinical practice: current approaches and challenges. *Pharmaceutics* 2019;11(11).
18. Parekkadan B, Milwid JM. Mesenchymal stem cells as therapeutics. *Annu Rev Biomed Eng*. 2010;12:87-117. [in English]. https://doi.org/10.1146/annurev-bioeng-070909-105309
19. Egger D, Tripisciano C, Weber V, et al. Dynamic cultivation of mesenchymal stem cell aggregates. *Bioengineering (Basel)*. 2018;5(2).
20. Pittenger MF, Discher DE, Peault BM, et al. Mesenchymal stem cell perspective: cell biology to clinical progress. *NPJ Regen Med*. 2019;4:22. https://doi.org/10.1038/s41536-019-0083-6
21. Levy O, Kuai R, Siren EMJ, et al. Shattering barriers toward clinically meaningful MSC therapies. *Sci Adv*. 2020;6(30):eaba6884.

22. Saeedi P, Halabian R, Imani Fooladi AA. A revealing review of mesenchymal stem cells therapy, clinical perspectives and modification strategies. *Stem Cell Investig*. 2019;6:34. https://doi.org/10.21037/sci.2019.08.11
23. Placzek MR, Chung IM, Macedo HM, et al. Stem cell bioprocessing: fundamentals and principles. *J R Soc Interface*. 2009;6(32):209-232. https://doi.org/10.1098/rsif.2008.0442
24. Murphy KC, Fang SY, Leach JK. Human mesenchymal stem cell spheroids in fibrin hydrogels exhibit improved cell survival and potential for bone healing. *Cell Tissue Res*. 2014;357(1):91-99. https://doi.org/10.1007/s00441-014-1830-z
25. Yamaguchi Y, Ohno J, Sato A, et al. Mesenchymal stem cell spheroids exhibit enhanced in-vitro and in-vivo osteoregenerative potential. *BMC Biotechnol*. 2014;14:105. https://doi.org/10.1186/s12896-014-0105-9
26. Petrenko Y, Sykova E, Kubinova S. The therapeutic potential of three-dimensional multipotent mesenchymal stromal cell spheroids. *Stem Cell Res Ther*. 2017;8(1):94.
27. Sart S, Tsai AC, Li Y, et al. Three-dimensional aggregates of mesenchymal stem cells: cellular mechanisms, biological properties, and applications. *Tissue Eng Part B Rev*. 2014;20(5):365-380. https://doi.org/10.1089/ten.TEB.2013.0537
28. Bartosh TJ, Ylostalo JH, Mohammadipoor A, et al. Aggregation of human mesenchymal stromal cells (MSCs) into 3D spheroids enhances their antiinflammatory properties. *Proc Natl Acad Sci USA*. 2010;107(31):13724-13729. https://doi.org/10.1073/pnas.1008117107
29. Frith JE, Thomson B, Genever PG. Dynamic three-dimensional culture methods enhance mesenchymal stem cell properties and increase therapeutic potential. *Tissue Eng Part C Methods* 2010;16(4):735-749. https://doi.org/10.1089/ten.TEC.2009.0432
30. Cha JM, Park H, Shin EK, et al. A novel cylindrical microwell featuring inverted-pyramidal opening for efficient cell spheroid formation without cell loss. *Biofabrication* 2017;9(3). [in English]
31. Cha JM, Shin EK, Sung JH, et al. Efficient scalable production of therapeutic microvesicles derived from human mesenchymal stem cells. *Sci Rep*. 2018;8(1):1171. https://doi.org/10.1038/s41598-018-19211-6
32. Ginestet C. ggplot2: elegant graphics for data analysis. *J R Stat Soc a Stat*. 2011;174:245-245. [in English]
33. Cao R, Eriksson A, Kubo H, et al. Comparative evaluation of FGF-2-, VEGF-A-, and VEGF-C-induced angiogenesis, lymphangiogenesis, vascular fenestrations, and permeability. *Circ Res*. 2004;94(5):664-670. https://doi.org/10.1161/01.RES.0000118600.91698.BB
34. Murakami M, Simons M. Fibroblast growth factor regulation of neovascularization. *Curr Opin Hematol*. 2008;15(3):215-220. https://doi.org/10.1097/MOH.0b013e3282f97d98
35. Farberov S, Basavaraja R, Meidan R. Thrombospondin-1 at the crossroads of corpus luteum fate decisions. *Reproduction* 2019;157(3):R73-R83. [in English]. https://doi.org/10.1530/REP-18-0530
36. Isenberg JS, Roberts DD. Thrombospondin-1 in maladaptive aging responses: a concept whose time has come. *Am J Physiol Cell Physiol*. 2020;319(1):C45-C63. https://doi.org/10.1152/ajpcell.00089.2020
37. Price MA, Colvin Wanshura LE, Yang J, et al. CSPG4, a potential therapeutic target, facilitates malignant progression of melanoma. *Pigment Cell Melanoma Res* 2011;24(6):1148-1157. https://doi.org/10.1111/j.1755-148X.2011.00929.x
38. Wang J, Svendsen A, Kmiecik J, et al. Targeting the NG2/CSPG4 proteoglycan retards tumour growth and angiogenesis in preclinical models of GBM and melanoma. *PLoS One*. 2011;6(7):e23062. https://doi.org/10.1371/journal.pone.0023062
39. Bignon M, Pichol-Thievend C, Hardouin J, et al. Lysyl oxidase-like protein-2 regulates sprouting angiogenesis and type IV collagen assembly in the endothelial basement membrane. *Blood* 2011;118(14):3979-3989. https://doi.org/10.1182/blood-2010-10-313296
40. Magnusson PU, Looman C, Ahgren A, et al. Platelet-derived growth factor receptor-beta constitutive activity promotes angiogenesis in vivo and in vitro. *Arterioscler Thromb Vasc Biol*. 2007;27(10):2142-2149. https://doi.org/10.1161/01.ATV.0000282198.60701.94
41. Dulak J, Loboda A, Zagorska A, et al. Complex role of heme oxygenase-1 in angiogenesis. *Antioxid Redox Signal*. 2004;6(5):858-866.
42. Chetty C, Lakka SS, Bhoopathi P, et al. MMP-2 alters VEGF expression via alphaVbeta3 integrin-mediated PI3K/AKT signaling in A549 lung cancer cells. *Int J Cancer*. 2010;127(5):1081-1095. https://doi.org/10.1002/ijc.25134
43. Lee H, Chang KW, Yang HY, et al. MT1-MMP regulates MMP-2 expression and angiogenesis-related functions in human umbilical vein endothelial cells. *Biochem Biophys Res Commun*. 2013;437(2):232-238. https://doi.org/10.1016/j.bbrc.2013.06.046
44. Quintero-Fabian S, Arreola R, Becerril-Villanueva E, et al. Role of matrix metalloproteinases in angiogenesis and cancer. *Front Oncol*. 2019;9:1370. https://doi.org/10.3389/fonc.2019.01370
45. Wu BT, Wen SH, Hwang SP, et al. Control of Wnt5b secretion by Wntless modulates chondrogenic cell proliferation through fine-tuning fgf3 expression. *J Cell Sci*. 2015;128(12):2328-2339. https://doi.org/10.1242/jcs.167403
46. Nie X, Liu H, Liu L, et al. Emerging roles of wnt ligands in human colorectal cancer. *Front Oncol*. 2020;10:1341. https://doi.org/10.3389/fonc.2020.01341
47. Minder P, Zajac E, Quigley JP, et al. EGFR regulates the development and microarchitecture of intratumoral angiogenic vasculature capable of sustaining cancer cell intravasation. *Neoplasia* 2015;17(8):634-649. https://doi.org/10.1016/j.neo.2015.08.002
48. Mori S, Hatori N, Kawaguchi N, et al. The integrin-binding defective FGF2 mutants potently suppress FGF2 signalling and angiogenesis. *Biosci Rep*. 2017;37(2).
49. Lee YJ, Lee HJ, Choi SH, et al. Soluble HSPB1 regulates VEGF-mediated angiogenesis through their direct interaction. *Angiogenesis* 2012;15(2):229-242. [in English]. https://doi.org/10.1007/s10456-012-9255-3
50. Wordinger RJ, Fleenor DL, Hellberg PE, et al. Effects of TGF-beta2, BMP-4, and gremlin in the trabecular meshwork: implications for glaucoma. *Invest Ophthalmol Vis Sci*. 2007;48(3):1191-1200. https://doi.org/10.1167/iovs.06-0296
51. Wang Y, He T, Liu J, et al. Synergistic effects of overexpression of BMP2 and TGFbeta3 on osteogenic differentiation of bone marrow mesenchymal stem cells. *Mol Med Rep*. 2016;14(6):5514-5520. https://doi.org/10.3892/mmr.2016.5961
52. Muraoka N, Shum L, Fukumoto S, et al. Transforming growth factor-beta3 promotes mesenchymal cell proliferation and angiogenesis mediated by the enhancement of cyclin D1, Flk-1, and CD31 gene expression during CL/Fr mouse lip fusion. *Birth Defects Res A Clin Mol Teratol*. 2005;73(12):956-965. https://doi.org/10.1002/bdra.20191
53. Aenlle KK, Curtis KM, Roos BA, et al. Hepatocyte growth factor and p38 promote osteogenic differentiation of human mesenchymal stem cells. *Mol Endocrinol*. 2014;28(5):722-730. https://doi.org/10.1210/me.2013-1286
54. Xin X, Yang S, Ingle G, et al. Hepatocyte growth factor enhances vascular endothelial growth factor-induced angiogenesis in vitro and in vivo. *Am J Pathol*. 2001;158(3):1111-1120. https://doi.org/10.1016/S0002-9440(10)64058-8
55. Gilbert RWD, Vickaryous MK, Viloria-Petit AM. Signalling by transforming growth factor beta isoforms in wound healing and tissue regeneration. *J Dev Biol* 2016;4(2).
56. Wang W, Rigueur D, Lyons KM. TGFbeta signaling in cartilage development and maintenance. *Birth Defects Res C Embryo Today*. 2014;102(1):37-51. https://doi.org/10.1002/bdrc.21058
57. Hu X, Zhang P, Xu Z, et al. GPNMB enhances bone regeneration by promoting angiogenesis and osteogenesis: potential role for tissue engineering bone. *J Cell Biochem*. 2013;114(12):2729-2737. https://doi.org/10.1002/jcb.24621
58. Prieto DMC, Cheng YS, Chang CC, et al. Direct integrin binding to insulin-like growth factor-2 through the C-domain is required for insulin-like growth factor receptor type 1 (IGF1R) signaling [in English]. *PLoS One*. 2017;12(9).

59. Dacic S, Kalajzic I, Visnjic D, et al. Col1a1-driven transgenic markers of osteoblast lineage progression. *J Bone Miner Res*. 2001;16(7):1228-1236. https://doi.org/10.1359/jbmr.2001.16.7.1228
60. Rosset EM, Bradshaw AD. SPARC/osteonectin in mineralized tissue. *Matrix Biol*. 2016;52-54:78-87. https://doi.org/10.1016/j.matbio.2016.02.001
61. Lai CF, Bai S, Uthgenannt BA, et al. Four and half lim protein 2 (FHL2) stimulates osteoblast differentiation. *J Bone Miner Res*. 2006;21(1):17-28. https://doi.org/10.1359/JBMR.050915
62. Cornish J, Callon KE, Naot D, et al. Lactoferrin is a potent regulator of bone cell activity and increases bone formation in vivo. *Endocrinology* 2004;145(9):4366-4374. [in English]. https://doi.org/10.1210/en.2003-1307
63. Boden SD, Liu Y, Hair GA, et al. LMP-1, a LIM-domain protein, mediates BMP-6 effects on bone formation. *Endocrinology* 1998;139(12):5125-5134. https://doi.org/10.1210/endo.139.12.6392
64. Nakamura M, Sone S, Takahashi I, et al. Expression of versican and ADAMTS1, 4, and 5 during bone development in the rat mandible and hind limb. *J Histochem Cytochem*. 2005;53(12):1553-1562. https://doi.org/10.1369/jhc.5A6669.2005
65. Kanamoto T, Mizuhashi K, Terada K, et al. Isolation and characterization of a novel plasma membrane protein, osteoblast induction factor (obif), associated with osteoblast differentiation. *BMC Dev Biol*. 2009;9:70. https://doi.org/10.1186/1471-213X-9-70
66. Mao M, Thedens DR, Chang B, et al. The podosomal-adaptor protein SH3PXD2B is essential for normal postnatal development. *Mamm Genome*. 2009;20(8):462-475. [in English]. https://doi.org/10.1007/s00335-009-9210-9
67. Takarada T, Hinoi E, Nakazato R, et al. An analysis of skeletal development in osteoblast-specific and chondrocyte-specific runt-related transcription factor-2 (Runx2) knockout mice. *J Bone Miner Res*. 2013;28(10):2064-2069. https://doi.org/10.1002/jbmr.1945
68. Komori T. Regulation of proliferation, differentiation and functions of osteoblasts by Runx2. *Int J Mol Sci* . 2019;20(7).
69. Nistala H, Lee-Arteaga S, Smaldone S, et al. Extracellular microfibrils control osteoblast-supported osteoclastogenesis by restricting TGF{beta} stimulation of RANKL production. *J Biol Chem*. 2010;285(44):34126-34133. https://doi.org/10.1074/jbc.M110.125328
70. Choi YA, Lim J, Kim KM, et al. Secretome analysis of human BMSCs and identification of SMOC1 as an important ECM protein in osteoblast differentiation. *J Proteome Res*. 2010;9(6):2946-2956. [in English]. https://doi.org/10.1021/pr901110q
71. Ge G, Greenspan DS. BMP1 controls TGFbeta1 activation via cleavage of latent TGFbeta-binding protein. *J Cell Biol*. 2006;175(1):111-120. https://doi.org/10.1083/jcb.200606058
72. Mukherjee A, Rotwein P. Insulin-like growth factor-binding protein-5 inhibits osteoblast differentiation and skeletal growth by blocking insulin-like growth factor actions. *Mol Endocrinol*. 2008;22(5):1238-1250. https://doi.org/10.1210/me.2008-0001
73. Le Blanc, K, et al. HLA expression and immunologic properties of differentiated and undifferentiated mesenchymal stem cells. *Exp Hematol*. 2003; 31(10):890-896.
74. Kumar H, Ha DH, Lee EJ. et al. Safety and tolerability of intradiscal implantation of combined autologous adipose-derived mesenchymal stem cells and hyaluronic acid in patients with chronic discogenic low back pain: 1-year follow-up of a phase I study. *Stem Cell Res Ther*. 2017; 8:262. https://doi.org/10.1186/s13287-017-0710-3
75. Salamanna F, Sartori M, Brodano GB, et al. Mesenchymal stem cells for the treatment of spinal arthrodesis: from preclinical research to clinical scenario. *Stem Cells Int*. 2017; 2017:3537094. https://doi.org/10.1155/2017/3537094
76. Blanco JF, Villarón EM, Pescador D, et al. Autologous mesenchymal stromal cells embedded in tricalcium phosphate for posterolateral spinal fusion: results of a prospective phase I/II clinical trial with long-term follow-up. *Stem Cell Res Ther*. 2019;10(1):63. https://doi.org/10.1186/s13287-019-1166-4
77. Ahn J, Park EM, Kim BJ, et al. Transplantation of human Wharton's jelly-derived mesenchymal stem cells highly expressing TGFβ receptors in a rabbit model of disc degeneration. *Stem Cell Res Ther*. 2015;6:190.
78. Anderson L, Seilhamer J. A comparison of selected mRNA and protein abundances in human liver. *Electrophoresis* 1997;18(3-4):533-537. https://doi.org/10.1002/elps.1150180333
79. Chen C, Hou J, Tanner JJ, et al. Bioinformatics methods for mass spectrometry-based proteomics data analysis. *Int J Mol Sci* . 2020;21(8).
80. Albrektsson T, Johansson C. Osteoinduction, osteoconduction and osseointegration. *Eur Spine J*. 2001;10(Suppl 2):S96-101. https://doi.org/10.1007/s005860100282
81. Alford AI, Kozloff KM, Hankenson KD. Extracellular matrix networks in bone remodeling. *Int J Biochem Cell Biol*. 2015;65:20-31. https://doi.org/10.1016/j.biocel.2015.05.008
82. Park YL, Park K, Cha JM. 3D-Bioprinting strategies based on in situ bone-healing mechanism for vascularized bone tissue engineering. *Micromachines (Basel)*. 2021;12(3).
83. Adhami MD, Rashid H, Chen H, et al. Loss of Runx2 in committed osteoblasts impairs postnatal skeletogenesis. *J Bone Miner Res*. 2015;30(1):71-82. https://doi.org/10.1002/jbmr.2321
84. Roux BM, Cheng MH, Brey EM. Engineering clinically relevant volumes of vascularized bone. *J Cell Mol Med*. 2015;19(5):903-914. https://doi.org/10.1111/jcmm.12569
85. Li R, Nauth A, Gandhi R, et al. BMP-2 mRNA expression after endothelial progenitor cell therapy for fracture healing. *J Orthop Trauma*. 2014;28(Suppl 1):S24-S27. https://doi.org/10.1097/BOT.0000000000000071
86. Saleh FA, Whyte M, Genever PG. Effects of endothelial cells on human mesenchymal stem cell activity in a three-dimensional in vitro model. *Eur Cell Mater*. 2011;22:242-57; discussion 257. https://doi.org/10.22203/ecm.v022a19
87. Wang J, Ye Y, Tian H, et al. In vitro osteogenesis of human adipose-derived stem cells by coculture with human umbilical vein endothelial cells. *Biochem Biophys Res Commun*. 2011;412(1):143-149. https://doi.org/10.1016/j.bbrc.2011.07.062
88. Almubarak S, Nethercott H, Freeberg M, et al. Tissue engineering strategies for promoting vascularized bone regeneration. *Bone* 2016;83:197-209. https://doi.org/10.1016/j.bone.2015.11.011
89. Martino MM, Briquez PS, Maruyama K, et al. Extracellular matrix-inspired growth factor delivery systems for bone regeneration. *Adv Drug Deliv Rev*. 2015;94:41-52. https://doi.org/10.1016/j.addr.2015.04.007
90. Santos MI, Reis RL. Vascularization in bone tissue engineering: physiology, current strategies, major hurdles and future challenges. *Macromol Biosci*. 2010;10(1):12-27. https://doi.org/10.1002/mabi.200900107
91. Santos MI, Unger RE, Sousa RA, et al. Crosstalk between osteoblasts and endothelial cells co-cultured on a polycaprolactone-starch scaffold and the in vitro development of vascularization. *Biomaterials* 2009;30(26):4407-4415. https://doi.org/10.1016/j.biomaterials.2009.05.004
92. Ancans J. Cell therapy medicinal product regulatory framework in Europe and its application for MSC-based therapy development. *Front Immunol*. 2012;3. [in English]
93. Man K, Brunet MY, Jones MC, et al. Engineered extracellular vesicles: tailored-made nanomaterials for medical applications. *Nanomaterials (Basel)*. 2020;10(9
94. Ten Ham RMT, Hoekman J, Hovels AM, et al. Challenges in advanced therapy medicinal product development: a survey among companies in Europe. *Mol Ther Methods Clin Dev*. 2018;11:121-130. https://doi.org/10.1016/j.omtm.2018.10.003
95. de Wilde S, Veltrop-Duits L, Hoozemans-Strik M, et al. Hurdles in clinical implementation of academic advanced therapy medicinal products: a national evaluation. *Cytotherapy*. 2016;18(6):797-805. https://doi.org/10.1016/j.jcyt.2016.02.010

96. Jin HJ, Bae YK, Kim M, et al. Comparative analysis of human mesenchymal stem cells from bone marrow, adipose tissue, and umbilical cord blood as sources of cell therapy. *Int J Mol Sci*. 2013;14(9):17986-18001. [in English]. https://doi.org/10.3390/ijms140917986
97. Dominici M, Le Blanc K, Mueller I, et al. Minimal criteria for defining multipotent mesenchymal stromal cells. The International Society for Cellular Therapy position statement. *Cytotherapy*. 2006;8(4):315-317. https://doi.org/10.1080/14653240600855905
98. Radrizzani M, Soncin S, Bolis S, et al. Quality control assays for clinical-grade human mesenchymal stromal cells: validation strategy. *Methods Mol Biol*. 2016;1416:339-356. https://doi.org/10.1007/978-1-4939-3584-0_20
99. Guidance for FDA reviewers and sponsors. Available at https://www.fda.gov/media/73624/download. Accessed April 2008.
100. Zhao J, Wang J, Dang J, et al. A preclinical study-systemic evaluation of safety on mesenchymal stem cells derived from human gingiva tissue. *Stem Cell Res Ther*. 2019;10(1):165. https://doi.org/10.1186/s13287-019-1262-5